

STATE OF CALIFORNIA • DEPARTMENT OF TRANSPORTATION
TECHNICAL REPORT DOCUMENTATION PAGE
 TR-0003 (REV 04/2024)

1. REPORT NUMBER CA25-3785	2. GOVERNMENT ASSOCIATION NUMBER	3. RECIPIENT'S CATALOG NUMBER
4. TITLE AND SUBTITLE Assessment of Paved Road Dust Emissions (Road Dust) Modeling		5. REPORT DATE April 2025
		6. PERFORMING ORGANIZATION CODE N/A
7. AUTHOR Francesca Hopkins, Roya Bahreini, and Akula Venkatram		8. PERFORMING ORGANIZATION REPORT NO. N/A
9. PERFORMING ORGANIZATION NAME AND ADDRESS Department of Mechanical Engineering Bourns Hall A342 900 University Ave. University of California, Riverside Riverside, CA 92521		10. WORK UNIT NUMBER N/A
		11. CONTRACT OR GRANT NUMBER
12. SPONSORING AGENCY AND ADDRESS California Department of Transportation (Caltrans) Division of Research, Innovation and System Information, MS-83 1727 30th Street Sacramento, CA 95816		13. TYPE OF REPORT AND PERIOD COVERED Final Report
		14. SPONSORING AGENCY CODE N/A

15. SUPPLEMENTARY NOTES

16. ABSTRACT

Under this project a novel road dust collection system has been designed that utilizes a modified van with a vacuum collection system that samples road dust on freeways. The project has also developed a new mechanistic model for particulate matter (PM) emission estimates as an alternative approach to the EPA's AP-42 model. The test for the road dust collection system has been conducted in a range of traffic flows from 1000 vehicles per hour to 14,000 vehicles per hour in the State Highway System. The geographic scope of the study occurred in CA-91, CA-60, CA 71, CA 55, I-15, I-215 freeways across 3 counties of southern California. Finally, the project applied the mechanistic model to the collected road dust samples. The van-based road dust collection system effectively sampled road dust on freeways, without disrupting traffic. Further, the researchers demonstrated the utility of the novel mechanistic model, determining the quantity, distribution and additional characteristics of road dust in the test area. The model provides comparable PM emissions estimates to the EPA AP-42 model and may be more broadly applicable to a wider range of conditions, including high traffic. Road dust is a significant pollutant of concern, and this research expanded the state of knowledge regarding how to assess it. The results of this project provide Caltrans and other regulatory agencies a new, efficient, and scalable method for assessing road dust's impact to air quality on highways and urban roads. If utilized further, this collection system and mechanistic model could extend Caltrans ability to test for road dust across the State Highway System and be used to develop a larger road dust model in the future. Such a model, that more fully characterizes road dust existing conditions and how the pollutant levels change, due to such factors as the increase of electric vehicles adoption, would provide Caltrans and other regulatory agencies a clearer understanding of the scope and scale of road dust, and when to consider regulatory adjustments. The model may also be developed further and potentially considered in the future as a Federal Equivalent Method regarding road dust emissions. That would improve Caltrans transportation project planning process, test new road dust mitigation methods, advance the Department's compliance with CEQA and NEPA more efficiently, and ultimately support improved public health.

17. KEY WORDS Road dust, particulate matter, PM10, PM2.5, AP-42 model, emission factor	18. DISTRIBUTION STATEMENT	
19. SECURITY CLASSIFICATION (of this report) Unclassified	20. NUMBER OF PAGES 86	21. COST OF REPORT CHARGED

Reproduction of completed page authorized.



Assessment of Paved Road Dust Emissions (Road Dust) Modeling

UCR/ME-80014-MR-2-R2

Caltrans Contract # 65A906

Prepared for:

California Department of Transportation

April 22, 2025

Principal Investigators:

Francesca Hopkins; Roya Bahreini; Akula Venkatram

Department of Mechanical Engineering

University of California, Riverside

Riverside, CA 92521



DISCLAIMER

This document is disseminated in the interest of information exchange. The contents of this report reflect the views of the authors who are responsible for the facts and accuracy of the data presented here. The contents do not necessarily reflect the official views or policies of the State of California. This publication does not constitute a standard, specification, or regulation. This report does not constitute an endorsement by the California Department of Transportation of any product described herein.

ACKNOWLEDGEMENTS

We extend our gratitude to the California Department of Transportation (Caltrans) for their generous support of the work described in this report. In particular, we want to thank Dr. Simon Bisrat, Dr. Yoojoong Choi, and Daisy Laurino for their invaluable guidance on both technical and non-technical matters related to the project. We also acknowledge with appreciation the scientists from State and Federal Agencies who served on our Project Advisory Committee, offering constructive feedback throughout the course of this project.

The field measurements were made possible by a group of individuals and organizations whose valuable contributions are greatly appreciated. We thank UCR Graduate and Undergraduate Students for their dedication to learning new tasks, working as a team, putting in long hours and working both late nights and early mornings. Dr. Yifan Ding led the team of students that conducted the first phase of this project during which the mobile dust sampling system was developed. He also evaluated the applicability of the AP-42 model to high-traffic roads. Mr. Amir Saeidi and Ms. Tianyi Wang played the major role in extending the sampling to several highways and assisted in the development of the mechanistic model to estimate road dust emission factors.

We extend our gratitude to Dr. Ranga Rajan Thiruvengkatachari and Dr. Nidia Rojas Robles for their assistance with the laboratory setup. We also thank graduate students Bradley Ries and Michelle Carr for their efforts in field studies. Bradley Ries led field data collection, instrument calibration and maintenance, data analysis, and the related source apportionments efforts. Additionally, we are grateful to Hongpufan Huang, Olivia Halseth, Sergio Beltran, Kenneth Chew, Duong Bao Khanh, Christine Wang, Joseph Solano, Rafael Ponce De Leon, Jansen Lindrose, and Alex Melendres for their dedication in collecting field measurements and assisting the lab work.

We are especially grateful for the support from the South Coast Air Quality Management District staff, especially Mr. Rene Bermudez and Dr. Mohammad Sowlat, for allowing us to deploy instruments at their monitoring sites, lending us instruments, and providing us with valuable auxiliary data. Last, we acknowledge the National Science Foundation for support of the ASCENT measurements at Rubidoux which improved the quality of our source apportionment results during Phase 3.

EXECUTIVE SUMMARY

Emissions of particulate matter (PM) from roadways can be classified into two primary categories: exhaust emissions and non-exhaust emissions (NEE). Non-exhaust emissions, often referred to as re-suspended dust or road dust (RD), encompass a range of sources such as the mechanical wear of tires, brakes, vehicle components, road materials, and the re-suspension of particles into the atmosphere due to vehicle-induced and atmospheric turbulence (Casotti Rienda and Alves, 2021). Recent studies indicate that road dust currently accounts for at least 50% of PM concentrations in urban areas (Amato et al., 2014; Denier van der Gon et al., 2018). By 2035, this contribution is projected to rise to about 67% (Reid et al., 2016; OECD, 2020) as exhaust emissions decline due to vehicle turnover and heavier electric vehicles enter the fleet, increasing both tire wear and dust resuspension. The growing dominance of road dust in overall PM highlights the importance of accurately quantifying this source and addressing the associated uncertainties.

The currently used regulatory model to estimate the road dust is described in the “Compilation of Air Pollutant Emissions Factors” (AP-42). The current version of the AP-42 model is a semi-empirical equation based on two inputs: road surface silt loading sL , which refers to the fraction of surface dust with aerodynamic diameter below $75 \mu m$ (US EPA, 1995), and average weight of vehicles on the road (US EPA, 2011a). The model has been criticized (Venkatram, 1999) for yielding unreliable emission results and its lack of a mechanistic foundation. Furthermore, the procedures recommended by AP-42 for sampling silt loading on paved roads require manual collection of road surface materials using a vacuum cleaner (US EPA, 1993). This collection is impractical for high traffic roads, which is the reason that there are few measurements of silt loading or emission factors for roads with traffic volume of more than 10,000 vehicles/h.

To address the difficulty of collecting silt loading on high-traffic roads, this study, initiated in January 2022, designed a mobile dust collection system to measure silt loading on California freeways with varying traffic volumes. The mobile dust collection system used a VacuMaid GV30, 740-watt vacuum cleaner with a HEVB (**H**igh-**E**fficiency **V**acuum **B**ag) filter bag for dust collection. A brush, connected with a telescopic hollow tube to the vacuum cleaner, made contact with the road to collect dust. The system also included a Picarro G2401-m CO/CO₂ analyzer, a PurpleAir sensor to measure PM concentrations and a 2D-sonic anemometer with a thermistor to measure meteorological variables. In the fall of 2023, the tube connected to the brush was spring-loaded to ensure stable contact of the brush to the road. An electrically-driven dust sieving machine replaced the time-consuming manual sieving. A phone GPS tracked the vehicle's location required to compute the distance traveled on the path of the road where dust was collected.

Variables, such as friction velocity, derived from measurements with the 2D anemometer and thermistor were calibrated with direct measurements from the 3D anemometer to ensure that the meteorological measurements were adequate for the dispersion modeling used to estimate emission factors. PurpleAir sensors were also calibrated with a BAM 1020, a regulatory-grade instrument¹. Additionally, measures were implemented to control dust mass loss during silt loading measurements.

This mobile platform system was used in field studies at six highways and two city roads: sections of CA-91, CA-60, CA 71, CA 55, I-15, I-215 freeway, Chicago Avenue, and Iowa Avenue across 3 Counties of California. During the summers of 2023 and summer 2024, a total of 109 dust samples were collected from road surfaces. In summer

¹ BAM 1020 refers to a particular model of Beta Attenuation Monitor (BAM) that has been **approved by the U.S. Environmental Protection Agency (EPA) as a Federal Equivalent Method (FEM)** for measuring ambient particulate matter (PM). In general, Beta Attenuation Monitors use a small radioactive source and a filter tape to measure airborne particles in near-real time.

2023, 64 samples were collected from two highways, I-215 and CA-91, and two city roads, Iowa Ave, and Chicago Ave. In spring and summer 2024, 45 samples were collected at CA-91, CA-60, CA-71, CA-55, I-15, I-215 freeways, and Chicago Avenue and Iowa Avenue in Riverside.

The field experiments performed during 2023 and 2024 provided data sets that were used to develop a mechanistic model for PM emission factors as an alternative to the AP-42 model. The AP-42 model provides estimates of emission factors that are within a factor of 5 of the measurements made on highways when measured values of silt loading are inputs to the model. The mechanistic model yields emission factor estimates that compare well with those from the AP-42 model. The major advantage that the mechanistic model offers over the AP-42 model is that it is based on physical arguments, which suggests its applicability to a wider range of conditions. The second advantage is that its input can be readily quantified without making measurements that require impractical disruption of traffic. We realize that measurements of emission factors used in this exercise are overestimates of resuspended dust because they include brake and tire wear emissions. One estimate from Matthaios et al. (2022) indicates that road dust resuspension, brake wear, and tire wear account for 29.6%, 19.6%, and 16.4% of the PM_{10-2.5} mass respectively.

To help separate the contribution of crustal material of road dust from brake and tire wear emissions, elemental composition of PM₁₀ and PM_{2.5} were measured at two sites in eastern parts of the Los Angeles Basin (Ontario and Rubidoux, respectively) and a source apportionment model, namely the Positive Matrix Factorization or PMF, was employed. The PMF resolved 6-7 factors that describe the variability of the measurements, including “Resuspended Dust”, “Brake Wear”, and “Tire Wear” factors. Next, fractional contribution of the Resuspended Dust factor to several crustal elements along with the soil mass parameterization equation of the IMPROVE network (Pettijohn, 1975) was used to estimate only the crustal mass associated with the

Resuspended Dust factor. When compared with the total PM10 and PM2.5 mass concentrations, it was estimated that crustal materials sourced from upwind roads in LA Basin that experience vehicular traffic contribute to 15% of PM10 and 12% of PM2.5.

These results from this project will greatly extend the ability of Caltrans and regulatory agencies in assessing the air quality impact of highways and city roads.

Table of Contents

1. Evaluation of the AP-42 Model and Development of a Mechanistic Model 1

1.1	Introduction and Objectives	1
1.2	The AP-42 Model.....	4
1.3	Field Studies.....	8
1.4	Computing Emission Factors	10
1.5	Modeling Emission Factors.....	11
1.6	Results	12
1.7	Discussion and Conclusions	17

2 Details of Field Studies and Instrumentation 22

2.1	Particle Concentration Measurement	23
2.2	Meteorological Measurements	25
2.3	Dust Collection and Silt Measurement System.....	27
2.3.1	Design of Dust Brush	27
2.3.2	Quality Control of Dust Collection	29
2.3.3	Dust Shaker	30
2.4	Improvements Made to Equipment During Field Studies.....	32
2.5	Traffic Flow Measurements	33

2.6	Field Studies.....	34
2.7	Evaluation of Emission Factor Estimates.....	36
2.8	Results	38
2.8.1	Concentration of PM _{2.5} , PM ₁₀ , and CO ₂	38
2.8.2	Meteorological Data.....	43
2.8.3	Traffic Count and Traffic Speed	45
2.8.4	Silt Loading.....	53
3	Analysis of Components of Road Dust.....	56
3.1	Field Sampling	56
3.2	Instrument Calibrations and QA/QC.....	58
3.3	Results	60
3.3.1	Elemental Composition Measurements.....	60
3.3.2	Elemental Spatial Distribution	61
3.3.3	Diurnal Profiles	67
3.3.4	Source Attributions	70
3.3.5	Overall Assessment of Contribution of Road Dust to PM ₁₀ and PM _{2.5}	76
3.3.6	Emission Factors of Road Crustal Material, Brake Wear, and Tire Wear ...	78
	References	82

Appendix A: Electronic Data Files for Dust Project..... 86

List of Figures

- Figure 1.1** Comparison of AP-42 model estimate with measured values taken from US EPA (2011b). The left panel shows the model estimates paired in time and location with the corresponding measurements. The right panel compares the distribution of the model estimates with that of the measurements. The parallel lines about the one-to-one line mark a factor-of-two interval. 6
- Figure 1.2** Variation of EF with average speed and weight of the vehicle on the road. 8
- Figure 1.3** The left panel shows the locations of the city roads, and the right panel shows the freeways that were sampled..... 9
- Figure 1.4** The schematic of paths taken by mobile platform during field studies. "ML" stands for "Mobile Lab," with each number indicating a distinct measurement scenario described in Section 2 of this report..... 10
- Figure 1.5** Comparison of the cumulative distribution of the ratio of the measured to the modeled PM10 emission factor with the cumulative distribution of the lognormal distribution based on the logarithmic mean and standard deviation of the measured ratios. Model corresponds to the mechanistic model, Equation (1.5) 14
- Figure 1.6** Comparison of modeled EFs (mg/(vehicle miles traveled) with measurements made during 2023 and 2024. The top panels refer model to estimates from the AP-42 model for PM2.5 and the bottom to PM10. The left panels plot paired model estimates and corresponding measurements, and the right to ranked modeled values versus ranked measurements. The model inputs are the measured values of silt loading in g/m² and average vehicle weight in short tons (2000 lb)..... 15
- Figure 1.7** Comparison of modeled EFs (mg/(vehicle miles traveled) with measurements made during 2023 and 2024. The top panels refer model to estimates from the $EF = k \cdot sL$ model for PM2.5 and the bottom to PM10. The left panels plot paired model estimates and corresponding measurements, and the right to ranked modeled values versus ranked measurements. The model inputs are the measured values of silt loading in g/m² 16
- Figure 1.8** Comparison of modeled EFs (mg/(vehicle miles traveled) with measurements made during 2023 and 2024. The top panels refer model for estimates from the $EF = k \cdot Weight / Vspd^2$ model for PM2.5 and the bottom to PM10. The left panels' plot paired model estimates and corresponding measurements, and the right to ranked modeled values versus ranked measurements. The model inputs are the average vehicle weight in short tons (2000 lb) and average vehicle speed in m/s..... 17
- Figure 1.9** Left panel shows the relationship between measured emission factors and silt loading measured on freeways. Right panel shows the cumulative frequency

<i>distribution of silt loading. Vertical line is the recommended default value of 15 mg/m²</i>	<i>19</i>
Figure 2.1 <i>The left panel shows the mobile platform with a 2-D sonic anemometer mounted at 3 m. The right panel shows the dust collection system mounted on the platform.</i>	<i>22</i>
Figure 2.2 <i>Correlation between PM_{2.5} and PM₁₀ measurements from BAM 1020 with those from PurpleAir.....</i>	<i>24</i>
Figure 2.3 <i>Experimental setup to compare meteorological parameters derived from the 3D sonic anemometer with those from the mobile platform meteorological sensors.</i>	<i>26</i>
Figure 2.4 <i>Comparison of meteorological variables measured with 3D sonic anemometers with modeled values derived from measurements with a 2D sonic anemometer and thermistor</i>	<i>27</i>
Figure 2.5 <i>Brush and the Section of brush that was trimmed to ensure contact with road.</i>	<i>28</i>
Figure 2.6 <i>a) Area vacuumed by the dust collection system, and b) Width of vacuumed area.</i>	<i>29</i>
Figure 2.7 <i>Dust sieving shaker.....</i>	<i>30</i>
Figure 2.8 <i>Silt Loading Measurement Process</i>	<i>31</i>
Figure 2.9 <i>(a) Particles bigger than 0.315 mm. (b) Particles between 0.315 mm and 0.15 mm. (c) Particles between 0.15 mm and 0.075 mm. (d) Particles between 0.075 mm and 0.0385 mm. (e) Particles smaller than 0.0385 mm.....</i>	<i>31</i>
Figure 2.10 <i>(a) Brush and tube attached to trailer (b) Details of attachment, (c) Components of attachment.....</i>	<i>32</i>
Figure 2.11 <i>Diagram of the Tracker Interface and Operation.....</i>	<i>34</i>
Figure 2.12 <i>Emission factors estimated with mobile platforms compared to those using data from stationary monitors.....</i>	<i>37</i>
Figure 3.1 <i>(a) location of the near-road sampling site in Ontario/Etiwanda; (b) location of the suburban sampling site in Rubidoux.....</i>	<i>57</i>
Figure 3.2 <i>Example of the nightly calibration response of Xact-625i to internal standards.....</i>	<i>59</i>
Figure 3.3 <i>Comparison of borrowed eBAM-PM₁₀ and SCAQMD-operated BAM-PM₁₀ instruments at Rubidoux during Phase 3.....</i>	<i>60</i>
Figure 3.4 <i>Distribution of the average concentration to uncertainty values reported for key elements in PM₁₀ and PM_{2.5} during Phase 1</i>	<i>61</i>

Figure 3.5 *Wind roses of wind speed, PM10, and several trace elements of PM10 (Fe and Si as tracers of crustal material, Ba as brake wear, and Zn and tire wear) for Phase 1 (Ontario/Etiwanda in Winter 2023)* 62

Figure 3.6 *Wind roses of PM2.5 and several trace elements of PM2.5 (Fe and Si as tracers of crustal material, Ba as brake wear, and Zn as tire wear) for Phase 1 (Ontario/Etiwanda in Winter 2023)* 62

Figure 3.7 *Wind rose of BC, NOx, and CO as markers of traffic- related emissions for Phase 1 (Ontario/Etiwanda in Winter 2023)* 63

Figure 3.8 *Box and whisker plots representing 10th, 25th, 50th, 75th, and 90th percentile values of PM10 and PM2.5 mass concentrations of Fe, Ca, Si, Ba, Zn, and Cu during Phase 1 (Ontario/Etiwanda, Winter 2023)* 63

Figure 3.9 *Wind roses of wind speed and PM10 for Phase 2 (Ontario/Etiwanda in Summer 2023)* 64

Figure 3.10 *Box and whisker plots representing 10th, 25th, 50th, 75th, and 90th percentile values of PM10 and PM2.5 mass concentrations of Fe, Ca, Si, Ba, Zn, and Cu during Phase 2 (Ontario/Etiwanda, Summer 2023). Data suggest the switching inlet valve was not working properly during this phase* 65

Figure 3.11 *Wind rose of wind speed and PM10 for Phase 3 (Rubidoux in Summer 2023)* 66

Figure 3.12 *Wind rose of BC, NOx, and CO as markers of traffic- related emissions for Phase 3 (Rubidoux in Summer 2023)* 66

Figure 3.13 *Box and whisker plots representing 10th, 25th, 50th, 75th, and 90th percentile values of PM10 and PM2.5 mass concentrations of Fe, Ca, Si, Ba, Zn, and Cu during Phase 3 (Rubidoux in Summer 2023). PM2.5 statistics are based on the data collected only during the deployment of Xact- PM10 for consistency in comparison* 67

Figure 3.14 *Diurnal profiles of BC and several elements in PM10 (a) and PM2.5 (b) for Phase 1 (Ontario/Etiwanda in Winter 2023)* 68

Figure 3.15 *Diurnal profiles of PM2.5, PM10, BC, CO, and O₃ for Phase 3 (Rubidoux, in Summer 2023). PM10 data corresponds to the period of deployment of the Xact at Rubidoux (Aug. 25- Sep. 5, 2023) while other data are averages for Aug.- Sep. 2023.* 69

Figure 3.16 *Diurnal profiles of several elements in PM10 and PM2.5 during Phase 3 (Rubidoux, Summer)* 70

Figure 3.17 *Distribution of different PM10 and PM2.5 PMF solutions across different elements during Phase 1 (Ontario/Etiwanda, Winter)* 73

Figure 3.18 *Distribution of different PM10 and PM2.5 PMF solutions across different elements during Phase 3 (Rubidoux, Summer)* 75

Figure 3.19 *Diurnal profiles of PM₁₀, PM_{2.5}, and calculated crustal mass of PM₁₀ and PM_{2.5} during Phase 3 (Rubidoux, Summer)..... 78*

Figure 3.20 *Diurnal profiles of PM₁₀, CO, crustal mass of PM₁₀ and PM_{2.5} during Phase 3 (Rubidoux, Summer). Early morning background values are subtracted so that enhancements during morning rush hour (5-10 am) can be considered as the traffic related emissions 78*

List of Tables

Table 1.1 <i>Model Performance Statistics</i>	20
Table 2.1 <i>Comparisons of PM₁₀ and PM_{2.5} measurements between PurpleAir and FEM BAM 1020 instruments</i>	25
Table 2.2 <i>Equipment list for mobile platforms</i>	33
Table 2.3 <i>Summary of sampling information on roads</i>	35
Table 2.4 <i>Concentrations of PM_{2.5} and PM₁₀</i>	38
Table 2.5 <i>Concentration of CO₂</i>	42
Table 2.6 <i>Meteorological data</i>	43
Table 2.7 <i>Traffic conditions on different roads in 2023</i>	47
Table 2.8 <i>Traffic conditions on different roads in 2024</i>	51
Table 2.9 <i>Silt loading from different roads in 2024</i>	53
Table 3.1 <i>Summary of measurements for different phases of the project. ⁺ Data not available between Feb. 4-8, 2023. [*] Data suggests that the switching valve was not operating as designed</i>	58
Table 3.2 <i>Summary of Resuspended Dust attributions to Ca, Fe, Ti, and Si in PM₁₀ and PM_{2.5} PMF solutions during Phase 3 (Rubidoux, Summer)</i>	77

1 Evaluation of the AP-42 Model and Development of a Mechanistic Model

1.1 Introduction and Objectives

Particulate matter (PM), broadly categorized according to aerodynamic diameter into PM_{2.5} ($\leq 2.5 \mu\text{m}$) and PM₁₀ ($\leq 10 \mu\text{m}$), remains a focal point in air quality management because of its pronounced health impacts. Due to their small size, these particles can be inhaled deep into the respiratory tract, aggravating or even triggering respiratory ailments such as asthma and chronic obstructive pulmonary disease (COPD), and, in the case of PM_{2.5}, reaching the alveolar regions and entering the bloodstream (Pope and Dockery, 2006; Cohen et al., 2017). Chronic exposure is linked to reduced lung function, heightened cardiovascular risk, and increased mortality. This underscores the importance of mitigating PM emissions, particularly in urban environments.

A substantial fraction of urban PM₁₀ and PM_{2.5} concentrations arises from road traffic, encompassing both exhaust and non-exhaust emissions. While exhaust emissions stem directly from incomplete fuel combustion in internal combustion engines, non-exhaust sources include brake wear, tire wear, and the resuspension of road dust (Thorpe and Harrison, 2008; Pant and Harrison, 2013). Resuspension occurs when vehicle-induced turbulence and mechanical friction lift settled particles back into the air. These road dust particles can contain a complex mix of soil-derived minerals, heavy metals from brake linings (e.g., copper, antimony), and rubber residues from tire wear (Amato et al., 2009). Meteorological factors such as wind speed, humidity, and precipitation also modulate resuspension rates, often making it highly variable across regions and seasons (Nicholson, 1988).

From a regulatory and planning perspective, accurate quantification of road dust emissions is critical for designing targeted mitigation strategies. In the United States, emissions inventories often employ the AP-42 emission factors published by the Environmental Protection Agency (EPA) alongside the MOVES (Motor Vehicle Emission Simulator) model to estimate both exhaust and non-exhaust PM contributions. These tools use empirical data and activity-based parameters (e.g., vehicle miles traveled, fleet composition, road type) to calculate emission inventories at local or regional scales. In Europe, the EMEP/EEA (European Monitoring and Evaluation Programme/European Environment Agency) Air Pollutant Emission Inventory Guidebook serves as a key reference for emission factors, supplemented by region-specific modeling tools such as COPERT (Computer Programme to Calculate Emissions from Road Transport) and HBEFA (Handbook Emission Factors for Road Transport) (Ntziachristos and Boulter, 2009). These comprehensive guides incorporate real-world measurements and research findings to refine emission estimates, acknowledging the contribution of local factors (traffic density, road condition, climate) and encouraging harmonized reporting across member states.

Amato et al., (2009) provides a review of the variety of methods that are in use to dust emissions from roads. In this paper, we focus on the AP-42 model, which is used in the US and several countries in Europe and Asia used to estimate emission factors for PM₁₀ and PM_{2.5} emissions from roads. Details of the model and its evaluation are described in the “Compilation of Air Pollutant Emissions Factors” (AP-42). U.S. Environmental Protection Agency (EPA) initially published in 1968. The model is routinely updated (US EPA 2011a). The current version of the AP-42 model is a semi-empirical equation based on two inputs: road surface silt loading (sL), which refers to the fraction of surface dust with aerodynamic diameter below $75 \mu m$ (US EPA 1993), and average weight of vehicles traveling on a road (US EPA 2011b).

The AP-42 model has been criticized (Venkatram 2000) for yielding unreliable emission results and its lack of a mechanistic foundation. The procedures recommended by AP-42 for sampling silt loading on paved roads require manual collection of road surface materials using a vacuum cleaner (US EPA 1993). This collection is impractical for high traffic roads, which is the reason that there are few measurements of silt loading or emission factors for roads with a traffic volume of more than 10000 vehicles/hr.

The primary goal of this research project summarized in this report is to develop a model for paved road dust emission factors that improves upon the current AP-42 model for estimating emission factors of road dust (PM₁₀ and PM_{2.5}) for California freeways with high traffic volume, which uses a default silt loading of 0.015 g/m^2 in the absence of measurements.

This objective was achieved by:

1. Developing a mobile platform that allowed measurement of the model inputs on high-traffic roads without the need for disrupting traffic flow.
2. Using the mobile platform to conduct field studies on several highways and roads in Southern California.
3. Using the data from these studies to evaluate the applicability of the AP-42 model to high-traffic roads.
4. Using the data to develop a mechanistic model for PM_{2.5} and PM₁₀ emission factors that improve upon the formulation of the AP-42 model and yields estimates of emission factors that compare well with those of the AP-42 model based on measurements of silt loading.
5. Using measurements of the chemical components of ambient PM₁₀ to separate dust emissions from the road from other contributing sources such as brake and tire wear.

This report consists of three chapters. In the first, we describe the evaluation of the AP-42 model and the development of the mechanistic model using the data collected in the field studies we conducted. This necessitates a brief description of the field studies and the associated data collection methods. In the second chapter of the report, we provide details of the development of the mobile platform that allowed measurements of silt loading and emission factors of PM_{2.5} and PM₁₀ on high-traffic roads. Chapter 3 describes the measurements of PM concentrations at an urban site and the analysis of the components of the concentrations of road dust to determine their origin.

1.2 The AP-42 Model

The current version of the emission factor for particulate matter emissions from paved roads is.

$$EF = k \times (sL)^{0.91} \times (Weight)^{1.02} \quad (1.1)$$

where EF is the particulate matter emission factor [$g/(veh \cdot mile)$], sL is the road surface silt loading [g/m^2], k is the particle size multiplier taken to be 0.25 and 1.00 for PM_{2.5} and PM₁₀ respectively, and $Weight$ is the average weight [short tons] of vehicles traveling on the road (US EPA, 2011a.). The empirical equation is based on 83 tests conducted on public and paved roads between 1983 and 2008. A technical memorandum from Caltrans (US EPA, 2011b) provides a description of the features of the data (most of the wording is taken directly from the report):

1. The equation is based on 83 road dust measurement tests with limited geographic coverage.
2. More than 70% of the measurement tests that support the equation were conducted on roadways at or near industrial facilities, and nearly two-thirds of the tests involved predominately medium-duty and heavy-duty vehicles. None of the tests include roadways in California.

3. Only 7 of the measurement tests involved vehicles traveling at 55 mph on freeways or expressways. Much of the test data are from roads with slow moving traffic and stop-and-go traffic. The data did **NOT** include the following information relevant to high-traffic roads:
 - low silt loading ($< 0.1 \text{ g/m}^2$, and especially $< 0.03 \text{ g/m}^2$)
 - high vehicle speed ($> 55 \text{ mph}$)
 - low fleet-average vehicle weight ($< 3 \text{ tons}$) with low vehicle speed ($< 35 \text{ mph}$)
4. About 25% of the measurement data that support the equation are from roadways with vehicle speeds less than 15 mph.
5. The current default silt loading value for freeways, 0.015 g/m^2 , lies outside the range of conditions that were considered in developing the paved road dust equation.
6. There is a significant data gap for road dust emission measurements of PM_{2.5}. Road dust emission factors for PM_{2.5} are scaled from PM₁₀ emission factors using an assumed particle size parameter (k). This approach assumes that the PM₁₀ and PM_{2.5} particle size multipliers reasonably represent the particle size distribution of California paved road dust.
7. The current EPA default value for the particle size parameter (k) for PM_{2.5} (0.25 g/VMT) is based on data collected on freeway and local roads in Denver, Raleigh, and Reno, and may not be representative of the PM_{2.5}/PM₁₀ ratio of paved road dust emissions in California.
8. The emission factors for PM₁₀ and PM_{2.5} were computed by subtracting modeled emissions of exhaust, brake, and tire (EBT) wear from the measured dust emissions. Thus, the AP-42 model reflects uncertainty in the modeled EBT emissions.

Figure 1.1 compares the PM10 emission factors presented in the AP-42 EPA report with estimates from Equation (1.1).

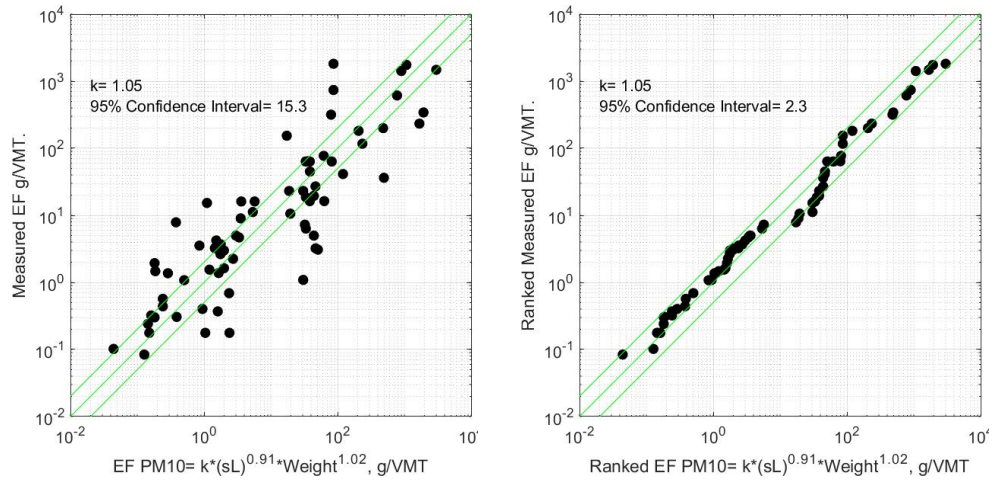


Figure 1.1 Comparison of AP-42 model estimate with measured values taken from US EPA (2011b). The left panel shows the model estimates paired in time and location with the corresponding measurements. The right panel compares the distribution of the model estimates with that of the measurements. The parallel lines about the one-to-one line mark a factor-of-two interval.

The model performance statistics presented here and in subsequent sections are computed by assuming that the measurements of emission factors are lognormally distributed to the modeled value. The parameter $k=1.05$ in the model is obtained by fitting model estimates to measurements so that the geometric mean of the ratios of the model estimates to measurements is unity. The 95% confidence interval is estimated from $s^{1.96/g}$ where s is the geometric ratio of the ratio of modeled to measured emission factors.

Figure 1.1 compares model estimates to corresponding observations in two ways. In the first, the model estimates are paired in time and location with the corresponding measurements. In the second approach, model estimates and measurements are ranked from low to high values before comparing them; this is equivalent to comparing the distributions of the two variables. There are good arguments (Venkatram et al., 2001; Perry et al., 2005) for estimating model uncertainty using distributions of model

estimates and corresponding observations rather than paired values when models are applied in a regulatory context. The question that this comparison asks is: Is the model capable of estimating the measured distribution of the variable to allow estimating the statistics required for regulatory decision-making?

The right panel of [Figure 1.1](#) shows that the scatter of the measured EFs about modeled values is relatively large, with an estimated 95% confidence interval of a factor of 15: 95% of the measured values are within a factor of 15 of a given model estimate. The scatter is reduced to a factor of 2.3, as seen in the right panel when the distributions are compared. Note that almost all the measured EFs are above 100 mg/VMT , which we will see is close to the maximum of those measured on high-traffic roads.

Because the model is empirical, the values of k in the expression depend on the data used to derive the model (Venkatram 2000). The fitted $k = 1.05$ is close to $k = 1.0$ recommended by the USEPA for the PM10 emission factor model.

[Figure 1.2](#) indicates that the EPA-compiled data corresponds to vehicle speeds of less than 25 mph, which is well below the average vehicle speeds on highways. Furthermore, 65% of the average vehicle weight included in the data set is over 3 tons, which is not representative of vehicles on highways. This focus on heavy vehicles traveling at low speeds is associated with a mean silt loading of over 20 g/VMT , which is (Rienda and Alves, 2021) well above values measured on most highways. It is clear that the data used to formulate the AP-42 model is of limited relevance to estimating emissions of PM from high-traffic highways. In the next section, we describe studies to fill this data gap.

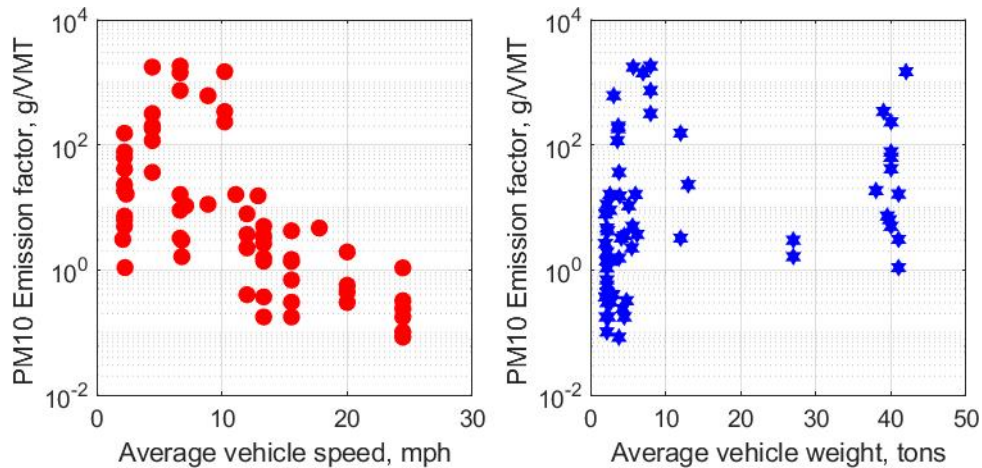


Figure 1.2 Variation of EF with average speed and weight of the vehicle on the road (US EPA, 2011b).

1.3 Field Studies

We overcame the problems associated with estimating PM emission factors from high traffic roads by developing a mobile platform that allowed us to measure silt loading, particulate concentrations, and meteorological variables without setting stationary monitors next to the highways that we studied. Here we provide a brief description of the system, the details of which are described in Chapter 2 of this report.

The mobile laboratory was equipped with PurpleAir PM monitors and one Picarro G2401-m In-flight Gas Concentration Analyzer CO/CO₂ gas concentration analyzer. The inlets for both the gas and PurpleAir PM monitors were mounted on the side door of the vehicle at an elevation of approximately 1.2 meters.

Meteorological information was measured with a 2-D sonic anemometer mounted on the mobile platform. A thermistor was mounted on the same tower where the sonic anemometer was mounted. The 2-D sonic anemometer measured 2-D winds, while the bead thermistor measured temperature, both at a frequency of 1 Hz.

The mobile dust collection system consisted of a brush connected to a VacuMaid GV30 central vacuum cleaner powered by 3.5 kW UPS (Expanded Uninterruptible Power Supply) powered. The brush, attached to a spring-loaded arm, was designed to keep

contact with the road as the mobile platform made transects. The dust collected by the system was then sieved to compute silt loading.

Sampling was conducted on six freeways and two city roads in Riverside, San Bernardino, and Orange County, California. The on-road field studies were conducted during the Summer 2023 and Spring 2024 on sections of CA-91, CA-60, CA-71, CA-55, I-15, I-215 freeways, Chicago Avenue, Iowa Avenue in 3 Counties of California, as shown in [Figure 1.3](#). The sampling was conducted on sections of roads that were 1.22 to 3.51 km long and widths ranging from 24 to 50 m.

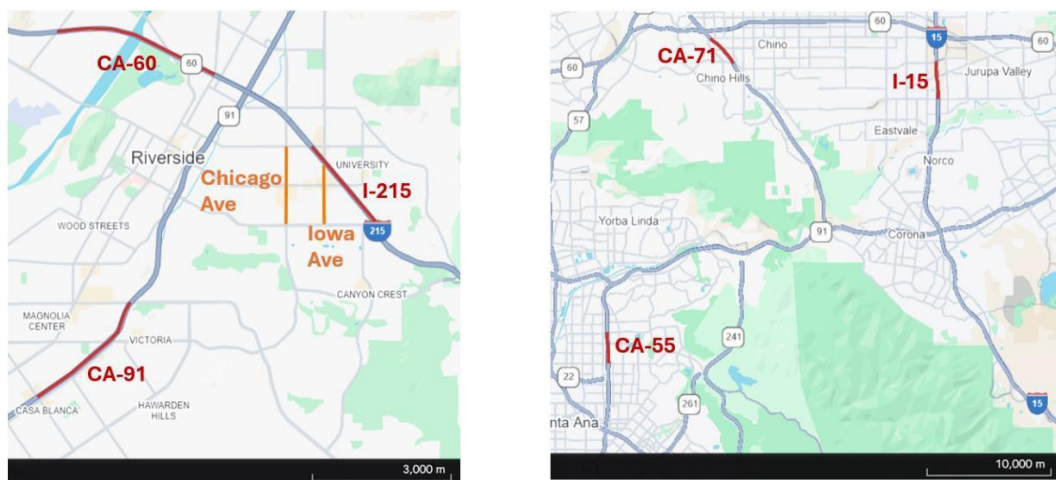


Figure 1.3 The left panel shows the locations of the city roads, and the right panel shows the freeways that were sampled.

A phone-based GPS tracked the vehicle's location and was used to compute the distance traveled by the van. The van was driven at speeds around 30 mph in the rightmost lane, ensuring that the brush was fully in contact with the ground for stable dust collection. A trailing vehicle observed the brush and provided additional safety. Dust samples were obtained from both freeway and local streets, with HEVB (**H**igh-**E**fficiency **V**acuum **B**ag) bags subsequently sent to the lab for weighing.

As shown in [Figure 1.4](#), in scenario 1 and 4, particulate concentration measurements were measured while the vehicle was in motion on the upwind and downwind sides of the road, followed by a stationary measurement for 10-15 minutes. This stationary setup allowed us to collect turbulence parameters, such as the standard deviation of the

vertical velocity σ_w and surface heat flux Q_o . Scenario 3 includes stationary measurements taken upwind, aiding in the determination of background concentrations and relevant meteorological variables such as wind direction and speed.

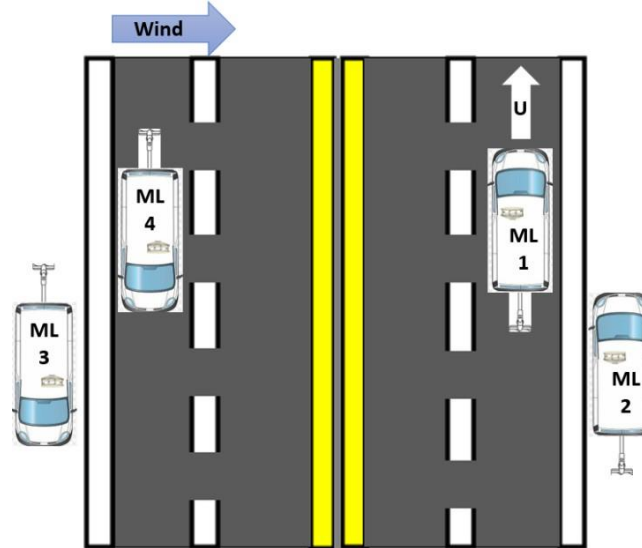


Figure 1.4 The schematic of paths taken by mobile platform during field studies. "ML" stands for "Mobile Lab," with each number indicating a distinct measurement scenario described in Section 2 of this report.

1.4 Computing Emission Factors

We used two methods to estimate emission factors for PM_{2.5} and PM₁₀, both of which are based on differences in concentrations of PM between the upwind and downwind side of a road. The governing equation is:

$$C = qD(\text{source receptor geometry, Meteorology}) \quad (1.2)$$

where ΔC is the concentration difference across the road, q ($g/(m \cdot s)$) is the emission rate of PM per unit length of the road, and D is a dispersion function that depends on source-receptor geometry and meteorological variables. Then the emission factor, EF (g/m) is given by:

$$EF = \frac{q}{T_r} \quad (1.3)$$

where T_r is the traffic flow rate (veh/s).

We computed D using two different models, a line source model similar to RLINE (Snyder et al. 2013) and a simplified version (Venkatram and Schulte 2018) that depends on a smaller set on input variables. The two models yielded results within 30% of each other, which is well within the factor of four uncertainty of the emission estimates. The simpler model is given by:

$$D = \sqrt{\frac{2}{\pi}} \frac{1}{W\sigma_w} \ln \left(1 + \frac{W\sigma_w}{h_o U \cos \theta} \right) \quad (1.4)$$

where W is the road width in [m], σ_w is the standard deviation of vertical velocity [m/s] measured by the mobile platform, U is the wind speed [m/s] observed on the mobile platform, h_o is the initial mixing height taken to be 2 m in this study, and θ is the angle between the normal to the road and the wind direction.

1.5 Modeling Emission Factors

We interpreted data from the field studies using three models. The first is the AP-42 model given by Equation (1.1). The second model assumes that the emission factor depends only on the silt loading.

The third model is based on the following mechanistic argument. Assume that moving vehicles only access a small fraction of the dust embedded on the road so that the emission rate of dust is determined by the frictional force applied by a vehicle on the road. Take the force applied as $\mu \cdot Weight$, where μ is a friction coefficient and $Weight = mg$ is the weight of the average vehicle on the road. This force acting over a distance d performs work given by $\mu \cdot Weight \cdot d$ which gives rise to particle emissions of $EF \cdot d$ with a kinetic energy that we assume is proportional to the average speed of the vehicle, $Vspd$. This energy balance results in the following equations:

$$k \cdot \mu \cdot Weight \cdot d = (EF) \cdot d \cdot (Vspd)^2 \quad (1.5)$$

$$EF = k \cdot \mu \cdot Weight / Vspd^2$$

where k is an empirical constant. Because the model, Equation (1.5), assumes that the surface material available for resuspension is not depleted by dust emissions, it is likely to provide an upper bound on the emission factor.

We explored various methods of estimating μ using digital photographs of the road surface. At this time, we have not found a method that accounts for the variability of the road surface. Our results are based on a constant value of μ , which is absorbed in the empirical constant k .

The CO₂ data from the Picarro instrument showed little correlation with the PM data. Consequently, the data was not used to estimate emission factors for PM_{2.5} and PM₁₀.

1.6 Results

As described earlier, the measurements of emission rate and silt loading on the roads were made by driving the mobile platform along the upwind and downwind sides of the road. This sampling path took roughly two to five minutes on each side of the road and was repeated about five times over an hour. These measurements were processed to estimate emission factors corresponding to each loop lasting about 20 minutes.

The three models that we evaluated are:

$$EF = k_1(sL)^{0.91}Weight^{1.02}$$

$$EF = k_2(sL) \tag{1.6}$$

$$EF = \frac{k_3 \cdot Weight}{(Vspd)^2}$$

The performance of the models is measured using the statistics of the residual ϵ defined by

$$\epsilon = \log(\text{measured } EF) - \log(\text{modeled } EF) \tag{1.7}$$

which assumes that the measured values are lognormally distributed about the model estimate. Figure 1.5 shows that this assumption is well supported by the data

corresponding to the mechanistic model, [Equation \(1.5\)](#). This agreement between the measured and theoretical distributions also holds for the other two models listed in [Equation \(1.5\)](#).

The empirical factor, k_i , that multiplies the function of input variables is computed by ensuring that the geometric mean of the ratios of the model estimate to corresponding measurement is unity. To illustrate this calculation, assume that the emission factor is given by one of the models in [Equation \(1.6\)](#)

$$EF = kf(sL, Weight, Vspd) \quad (1.8)$$

where f is any one of the forms in [Equation \(1.6\)](#). Then the following choice for k

$$k = \exp(\text{mean}(\log(\frac{\text{measured } EF}{f(sL,W)}))) \quad (1.9)$$

ensures that $m_g = \exp(\text{mean}(\epsilon)) = 1$ and also minimizes $\text{mean}(\epsilon^2)$ in [Equation \(1.7\)](#).

The geometric standard deviation $s_g = \exp(\text{standard deviation}(\epsilon))$ measures the performance of the model. The 95% confidence interval of the ratio of the modeled to measured emission factor is conservatively estimated as $s_g^{1.96}$. A 95% confidence interval of 5 implies that 95% of the observations corresponding to a given model estimate are expected to lie within an interval of 5 times the model estimate.

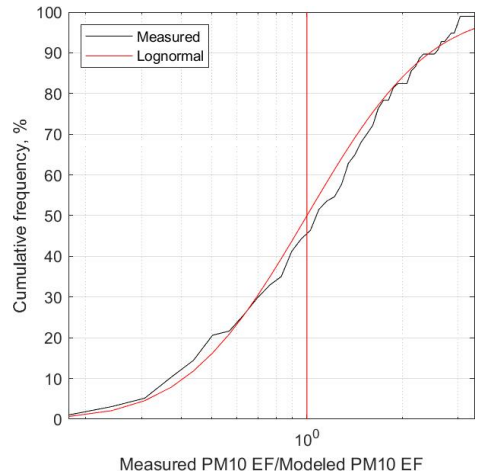


Figure 1.5 Comparison of the cumulative distribution of the ratio of the measured to the modeled PM10 emission factor with the cumulative distribution of the lognormal distribution based on the logarithmic mean and standard deviation of the measured ratios. Model corresponds to the mechanistic model, Equation (1.5)

Figure 1.6 shows the evaluation of the AP-42 model using the data collected during the summer of 2023 and the spring and summer of 2024. The plots of emission factors in the left panels show that the scatter of the measurements about model estimates is relatively large: the 95% confidence is 8 for PM10 and 5 for PM2.5. However, there is much better agreement between model estimates and measurements when the distributions of the two variables are compared by ranking them from low to high. The scatter of measurements about model estimates is less than a factor of two, which designated by the parallel lines that are above and below the one-to-one line.

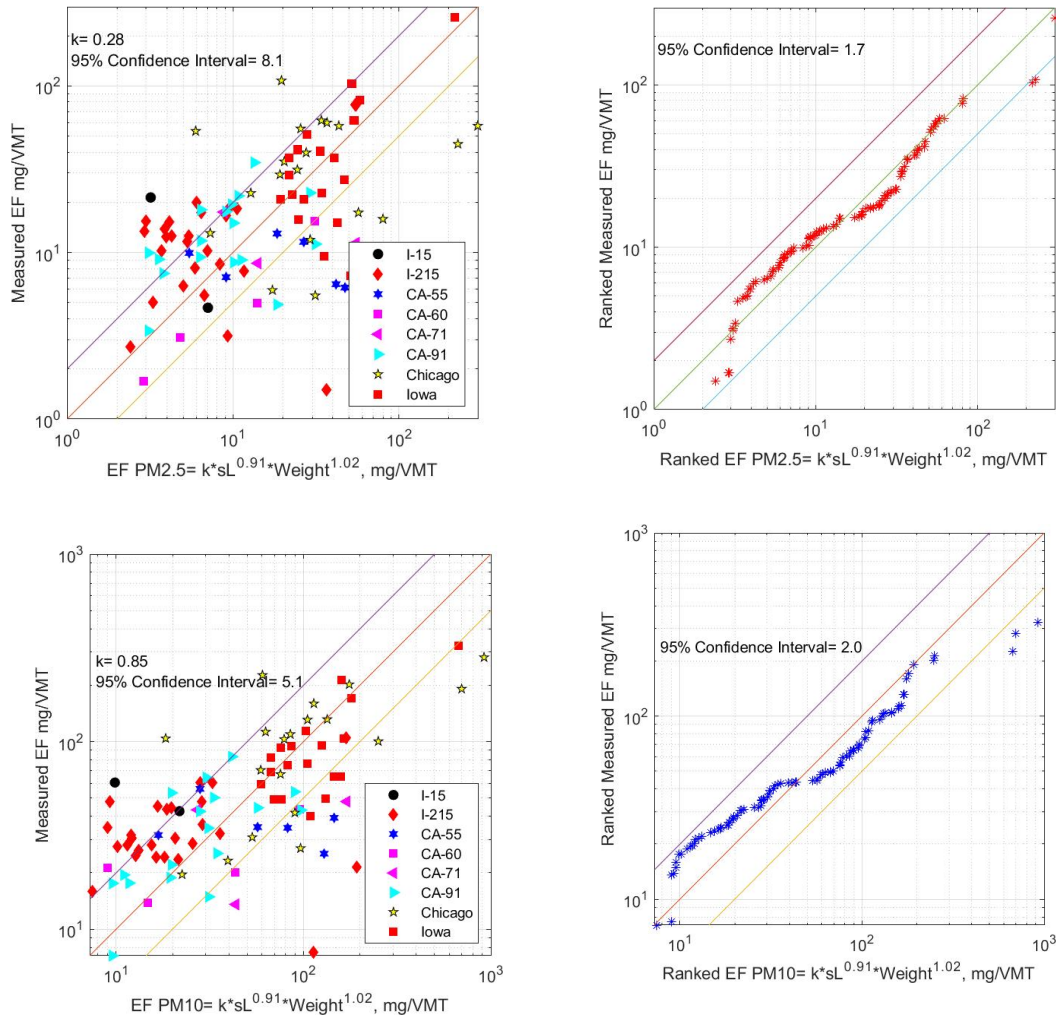


Figure 1.6 Comparison of modeled EFs ($mg/(vehicle\ miles\ traveled)$) with measurements made during 2023 and 2024. The top panels refer model to estimates from the AP-42 model for PM_{2.5} and the bottom to PM₁₀. The left panels plot paired model estimates and corresponding measurements, and the right to ranked modeled values versus ranked measurements. The model inputs are the measured values of silt loading in g/m^2 and average vehicle weight in short tons (2000 lb).

Figure 1.7 shows the results of evaluating a simpler version of the AP-42 model, $EF = k \cdot sL$, which does consider the average weight of vehicles. We see that although the paired comparison between model estimates and measurements is worse than that of the AP-42 model, the comparison of distributions is noticeably better. This suggests that measurements of just silt loading might provide adequate estimates of emission factors from a regulatory viewpoint.

Figure 1.8 shows the performance of the mechanistic model. The results on the left panels show that the model performs better than those based on silt loading when model estimates are paired with corresponding observations. However, the comparison of distributions of model estimates and measurements shows that the model overestimates concentrations at the high end of the modeled concentrations.

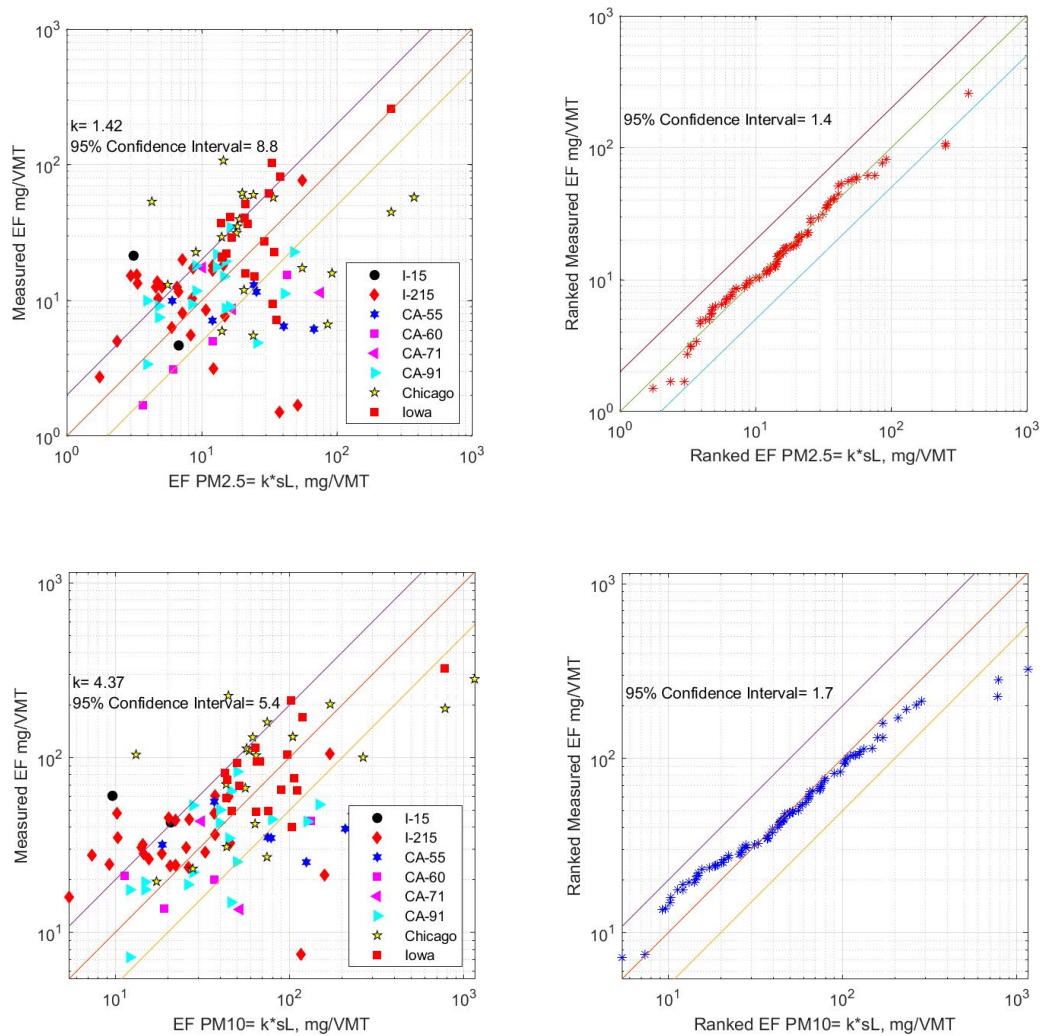


Figure 1.7 Comparison of modeled EFs ($\text{mg}/(\text{vehicle miles traveled})$) with measurements made during 2023 and 2024. The top panels refer model to estimates from the $\text{EF} = k \cdot \text{sL}$ model for $\text{PM}_{2.5}$ and the bottom to PM_{10} . The left panels plot paired model estimates and corresponding measurements, and the right to ranked modeled values versus ranked measurements. The model inputs are the measured values of silt loading in g/m^2 .

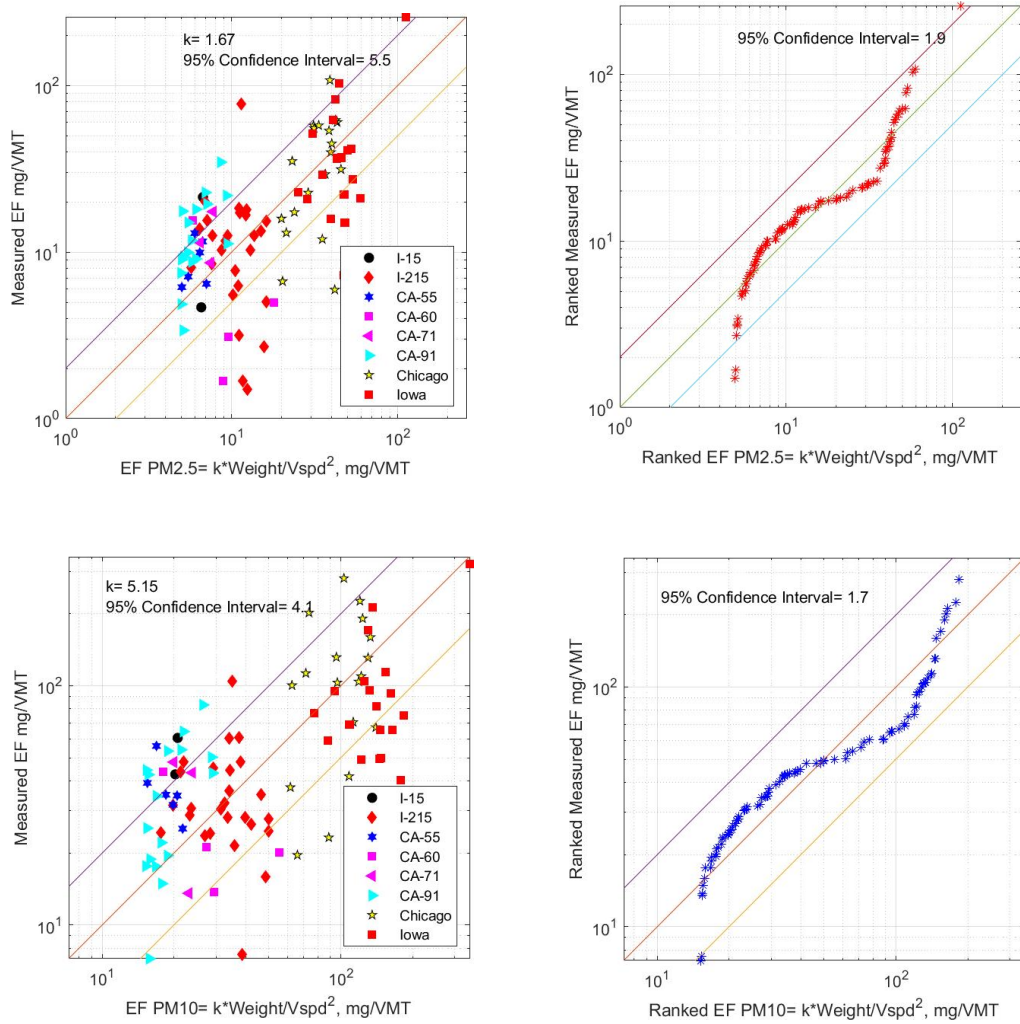


Figure 1.8 Comparison of modeled EFs (mg/(vehicle miles traveled)) with measurements made during 2023 and 2024. The top panels refer model for estimates from the $EF = k \cdot \text{Weight}/V\text{spd}^2$ model for PM_{2.5} and the bottom to PM₁₀. The left panels' plot paired model estimates and corresponding measurements, and the right to ranked modeled values versus ranked measurements. The model inputs are the average vehicle weight in short tons (2000 lb) and average vehicle speed in m/s.

1.7 Discussion and Conclusions

This study was motivated by the need to estimate emission factors for PM₁₀ and PM_{2.5} on high-traffic highways where it is difficult to deploy equipment to measure emission rates and inputs such as silt loading that are required in models for emission factors. The major results of the study described in this paper are:

1. Development and demonstration of a mobile platform system that enables the measurement of variables required to estimate emission factors of PM_{2.5} and PM₁₀ on high traffic roads.
2. Evaluation of the applicability of the AP-42 model to highways.
3. Formulation and evaluation of a mechanistic model to estimate emission factors of PM_{2.5} and PM₁₀ for high traffic roads.

Table 1.1 summarizes the statistics of the evaluation of three models using data collected from several highways in southern California. We see that when the estimates of emission factors from the AP-42 model are paired with corresponding measurements the scatter between the two variables is relatively large: the 95 % confidence interval ranges from 5 to 9. However, the distributions of modeled emission factors are within a factor of two of the measurements, suggesting that the model is adequate for regulatory applications. The empirical k factor of the original AP-42 model that multiplies the inputs of the emission factor for PM₁₀ is 0.85, which should be compared to the value of 1.05 corresponding to the data used by the USEPA to formulate the AP-42 model for low traffic roads.

We find that the emission factor is modeled well when expressed as a linear function of the silt loading. These results indicate that measured emission rates are strongly dependent on the measured silt loading. Because of the difficulty of measuring silt loading on highways, the AP-42 manual suggests a default value of 15 mg/m^2 when measurements are not available. Our measurements made on highways, shown in Figure 1.9 indicates that this value might lead to overestimates of emission factors because about 80% of the measured silt loading are less than the default value.

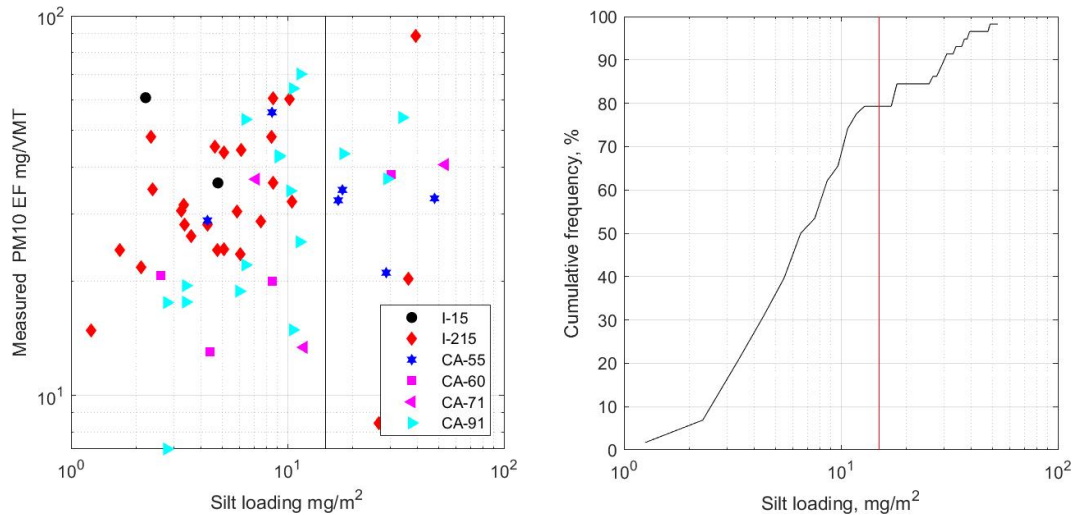


Figure 1.9 Left panel shows the relationship between measured emission factors and silt loading measured on freeways. Right panel shows the cumulative frequency distribution of silt loading. Vertical line is the recommended default value of 15 mg/m²

The ratio of the empirical factors, k , for PM_{2.5} and PM₁₀ is 0.33, which is higher than the 0.25 recommended in the AP-42 documentation. This ratio is approximately the same for all three models because they were fitted to measured emission factors that are all based on the same measurements of concentration differences of PM_{2.5} and PM₁₀ across the roads.

The mechanistic model yields emission factor estimates that improve upon those from the AP-42 model when model estimates are paired with corresponding measurements. However, the model shows a larger scatter than those of the silt-based models when the evaluation involves distributions of model estimates and measurements. This is an important issue in a regulatory context.

Table 1.1 Model Performance Statistics

Model	Species	<i>k</i>	95% confidence interval	95% confidence interval for distribution
<i>AP-42</i>	<i>PM2.5</i>	0.28	8.1	1.7
	<i>PM10</i>	0.85	5.1	2.0
<i>EF = k · sL</i>	<i>PM2.5</i>	1.42	8.8	1.4
	<i>PM10</i>	4.37	5.4	1.7
<i>EF = k · W/v²</i>	<i>PM2.5</i>	1.67	5.5	1.9
	<i>PM10</i>	5.15	4.1	1.7

In the absence of measurements of silt loading, the mechanistic model provides an estimate of the potential for dust emission: it increases with average weight of vehicles and decreases with the average speed of the traffic. Its input can be readily quantified without making measurements that require impractical disruption of traffic. Its formulation tells us that dust emissions can be reduced if the average speed of vehicles can be increased through traffic management.

All three emission-factor models are semi-empirical, meaning the “constants” in their equations are derived from observed data. Their reliability ultimately depends on independent validation by other researchers using separate datasets. Notably, the emission factors in this study span nearly two orders of magnitude, which suggests these models may be applicable beyond the specific highways from which the original data were collected. We realize that measurements of emission factors used in this exercise might be overestimates of resuspended dust because they include brake and

tire wear emissions. Specifically, Matthaios et al. (2022) estimate that road dust resuspension, brake wear, and tire wear account for 29.6%, 19.6%, and 16.4% of the PM10-2.5 mass, respectively.

2 Details of Field Studies and Instrumentation

As indicated earlier, we developed a mobile platform that allowed us to measure particulate concentrations and meteorological variables without setting up stationary monitors next to the highways that we studied.

All the instrumentation used in the field studies was mounted on the mobile platform, as shown in [Figure 2.1](#). The PM_{2.5} and PM₁₀ concentrations were measured with a PurpleAir monitor. Meteorological information was measured with a 2-D sonic anemometer and a thermistor. Dust from the road surface was collected with a brush mounted on a spring-loaded hollow arm, which was connected to a VacuMaid GV30 central vacuum cleaner powered with a 3.5 kW UPS (Expanded Uninterruptible Power Supply) rated at 740 watts.

The dust collected by the vacuum cleaner was sieved in the laboratory to obtain silt loading corresponding to particle diameters below $75 \mu m$. The following sections provide details of the instrumentation, and their deployment in the field.



Figure 2.1 *The left panel shows the mobile platform with a 2-D sonic anemometer mounted at 3 m. The right panel shows the dust collection system mounted on the platform.*

2.1 Particle Concentration Measurement

We measured PM concentrations using PurpleAir (PMS-6003) monitors, which consist of a pair of lasers scattering particle sensors, along with a Bosch BME688 sensor for measuring pressure, temperature, and humidity. It also features a Wi-Fi-enabled processor, enabling real-time data uploading to the cloud for immediate utilization. The PurpleAir SD card recording offers a minimum time resolution of approximately 2 minutes. However, the PurpleAir terminal provides the capability to retrieve raw data at a finer granularity of 1 second. PurpleAir monitors have not been used on mobile platforms in previous studies due to potential challenges in maintaining data quality. Section 4 describes steps that we have taken to maintain the integrity of the measurements from these instruments.

To eliminate the influence of the lab vehicle on the data, the PurpleAir sensor was secured with zip ties to the exterior of the driver's side door, approximately 1.5 meters above the ground. Once the field experiment began, the exact start and end times (to the second) were logged, and after the experiment concluded, data from the PurpleAir sensor and Picarro were exported to isolate the experimental time window for further recording and analysis.

The PurpleAir-II monitors were calibrated internally by co-locating them at the UCR Agricultural Operations (Ag-Ops). One PurpleAir monitor served as a reference monitor, and the other monitors were corrected based on its raw measurements. The reference PurpleAir was first calibrated with measurements taken with a BAM (Beta Attenuation Monitor) 1020 maintained by the South Coast Air Quality Management District (SCAQMD) at the Rubidoux, Riverside location.

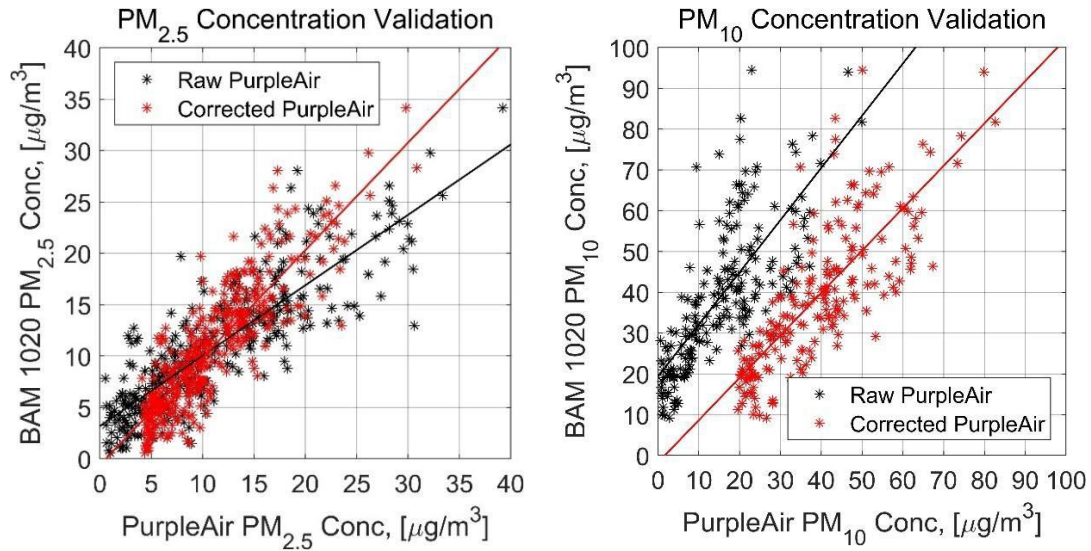


Figure 2.2 Correlation between $PM_{2.5}$ and PM_{10} measurements from BAM 1020 with those from PurpleAir.

The PurpleAir measurement was calibrated by regressing the PurpleAir measurements on the corresponding BAM measurements (Figure 2.2) using the equation suggested by Barkjohn et al. (2021)

$$BAM = s_1 \times PA_{reference} + s_2 \times T + s_3 \times RH + i \quad (2.1)$$

where $PA_{reference}$ is the reference PurpleAir measurements, BAM represents the BAM measurement ($\mu g/m^3$), T is the PurpleAir recorded air temperature in degrees Fahrenheit [$^{\circ}F$], RH is the PurpleAir measured relative humidity [%], s_1 , s_2 ($\mu g/(m^3 \cdot F)$), and s_3 ($\mu g/(m^3 \cdot \%)$) are determined using the non-negative least-squares method, which minimizes the square of the residual i between the reference measurements and raw measurements. Table 2.1 presents the results of the regression. Equation (2.1) was used to scale the measured PurpleAir PM concentration to obtain a magnitude that is consistent with the more accurate EBAM measurement.

Although the corrected PurpleAir measurements correlated well ($r^2 > 0.6$) with those from the FEM monitor, the scatter of the 2-minute-averaged measurements of PM between different PurpleAir instruments was larger than the concentration differences across a road, which was used to estimate emission rates of PM from roads.

Measurements with two DustTrak®s did not also provide the required precision. So, we decided to avoid the precision problem by using a single calibrated PurpleAir monitor to measure concentration differences across roads.

Table 2.1 Comparisons of PM_{10} and $PM_{2.5}$ measurements between PurpleAir and FEM BAM 1020 instruments

Particle Size		Slope	Intercept	s_1	s_2	s_3	R^2	m_g	Fact2
PM_{2.5}	Raw	0.7	3.2	1	0	0	0.73	0.95	87%
	Corrected	1.1	-0.6	0.67	0.05	0	0.76	1.1	92%
PM₁₀	Raw	1.3	19.4	1	0	0	0.55	0.32	23%
	Corrected	1.0	-1.7	1.32	0.25	0	0.6	1.06	96%

2.2 Meteorological Measurements

The meteorological information required to derive emission factors is based on a method that uses 2D wind information and high-frequency temperature data (Thiruvengkatachari et al., 2023). This method allowed us to obtain micrometeorological variables by parking the mobile platform next to a highway being studied. The more commonly used instrument, the 3D sonic anemometer, would have required setting up a tripod next to the road followed by careful leveling of the anemometer. This was impractical at most highway locations.

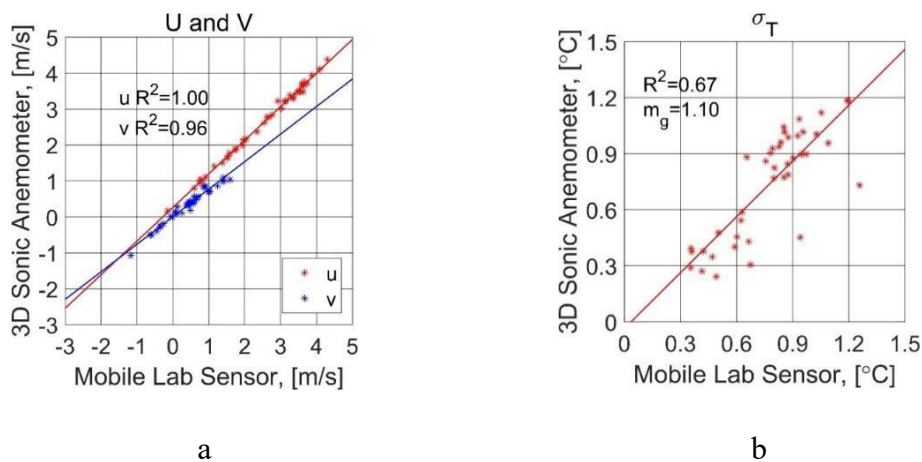
Our method of estimating micrometeorological variables was evaluated and calibrated with results from a Campbell Scientific CSAT3 3D 20 Hz sonic anemometer mounted on a stationary tower, as shown in Figure 2.3. The sonic anemometer was mounted at 3 m and 5 m on a tower.



Figure 2.3 Experimental setup to compare meteorological parameters derived from the 3D sonic anemometer with those from the mobile platform meteorological sensors.

The idling mobile lab was parked next to the 3D sonic anemometer for 8 hours each day to estimate the performance of the mobile platform observed meteorology as shown in Figure 2.4. The raw data from the sonic anemometer was then retrieved and processed to obtain 5-minute average micrometeorological parameters.

Figure 2.4 compares the meteorological measurements from the 3D sonic anemometer with those derived from measurements made on the mobile platform. Panels (c) and (d) show the performance of the mobile platform model in estimating the standard deviation of vertical speed, σ_w , and kinematic heat flux Q_o . The comparisons indicate that the meteorological parameters derived from the mobile platform are more than adequate as inputs to the dispersion model used to derive emission factors. Details are described in Thiruvengkatachari et al. (2023).



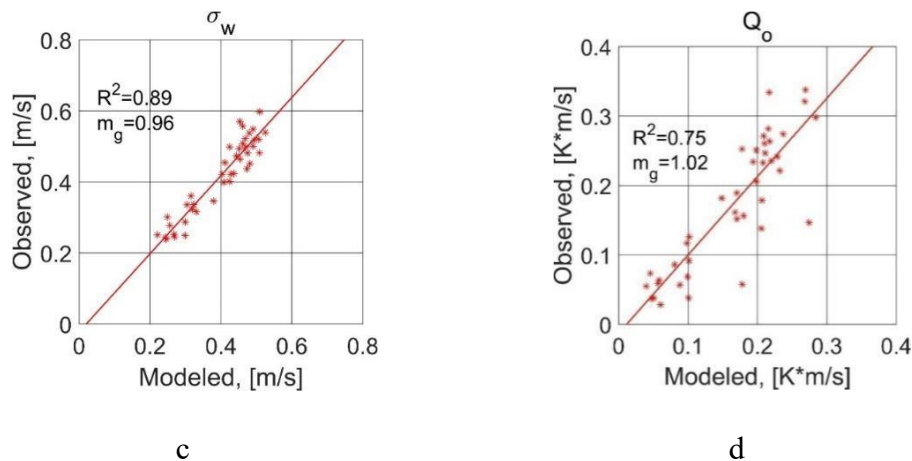


Figure 2.4 Comparison of meteorological variables measured with 3D sonic anemometers with modeled values derived from measurements with a 2D sonic anemometer and thermistor.

2.3 Dust Collection and Silt Measurement System

A mobile dust collection system was developed for a cargo van in the spring of 2023. The system used a 3.5 kW UPS to power a VacuMaid GV30 central vacuum cleaner, which features 740 max air watts and a High-Efficiency Vacuum Bag (HEVB) filter bag. A GPS tracker recorded the van's location to calculate travel distances. Inside the mobile lab, a Picarro G2401-m analyzer measured CO and CO₂ concentrations, while a PurpleAir sensor monitored PM concentrations on the driver-side door.

Dust from the road was collected with a telescopic hollow tube that connected the brush head to the vacuum cleaner. Straps secured the tube to the trailer and bungee cords were used to adjust brush position. A trailing vehicle monitored the brush to ensure that road conditions did not disable it, and that malfunctions of the equipment did not endanger the safety of other vehicles on the road.

2.3.1 Design of Dust Brush

Figure 2.5 shows the Cen-Tec Systems 34839 Vacuum brush to collect road dust. During preliminary experiments, we found that a significant portion of the dust was blocked by the rear bristles, preventing it from being sucked into the vacuum. This problem was solved by cutting off the rear bristles of the brush as shown in the red box

in [Figure 2.5](#). This ensured that all the dust in the area covered by the brush was collected into the vacuum.



Figure 2.5 *Brush and the Section of brush that was trimmed to ensure contact with road.*

Additionally, to ensure that dust particles were collected as thoroughly as possible into the vacuum, the brush was compressed by the spring-loaded arm on to the surface of the road. during the experiments. The contact area between the brush and the ground was not the original width of the brush (8 cm) multiplied by the travel distance, but rather the width of the bristles after they were compressed and spread out, multiplied by the travel distance.

[Figure 2.6](#) shows the width of the area vacuumed by the dust collection system. The width of the area, 11 cm, multiplied by the distance traveled by the mobile platform, is the effective area used to compute silt loading of the road.



Figure 2.6 a) Area vacuumed by the dust collection system, and b) Width of vacuumed area.

2.3.2 Quality Control of Dust Collection

After collecting the dust samples, the dust collection bags were transferred to the laboratory for measurement and analysis. Directly cutting open the dust bags and pouring the contents into the mesh would result in significant loss of fine dust particles. To minimize experimental errors, the dust collection bags were carefully prepared, with only the top portion being cut. The opening of the bag was placed at the bottom of a sealed bag, and the entire dust collection bag inverted. By gently tapping the dust bag, as much dust as possible was transferred into the sealed bag. Subsequently, a small 2 cm opening was made in the sealed bag to slowly pour the dust into the automatic sieving system.

There was always some fine residual dust left on the inner surface of the dust collection bags and the transfer bags after they were manually emptied. To control experimental errors, the empty dust collection bags and transfer bags were weighed in advance. After transferring the dust, the bags with residual dust were weighed again to determine the weight difference. We assumed that the diameter of the residual dust particles was less than 0.15 mm. After sieving (discussed next) was completed, this mass of residual dust

was distributed to the mass of particles below 0.15 mm using the sieved mass fractions as weighting factors.

2.3.3 Dust Shaker

To minimize errors and maximize throughput efficiency, an automatic dust sieving system was used separate the collected particulate matter in size ranges in [Figure 2.7](#). The system uses an electric vibrating sifter, which simulated the manual shaking process of the mesh. Because the standard sieve hole size of commercially available electric vibrating sieve machine sifter was too large to meet experimental requirements, a finer mesh was added to the sifter machine. The collected dust was then sieved sequentially through 0.315 mm, 0.15 mm, 0.075 mm, and 0.0385 mm of meshes. The dust per unit area with an aerodynamic diameter below 0.075 mm measured silt loading (sL).



Figure 2.7 *Dust sieving shaker.*

The automated sieving system is equipped sequentially with meshes of 0.315 mm, 0.15 mm, 0.075 mm, and 0.0385 mm. Each sample underwent a vibration screening process for 30-45 minutes, with duration depending on the initial dust sample weight. Details of the process used to determine silt mass are shown in the [Figure 2.8](#) and [Figure 2.9](#).

To prevent secondary loss of dust particles during transfer for weighing, the sieves were weighed together with the dust particles inside. The dust mass in each sieve was then determined by subtracting the previously measured empty sieve weight from this total.

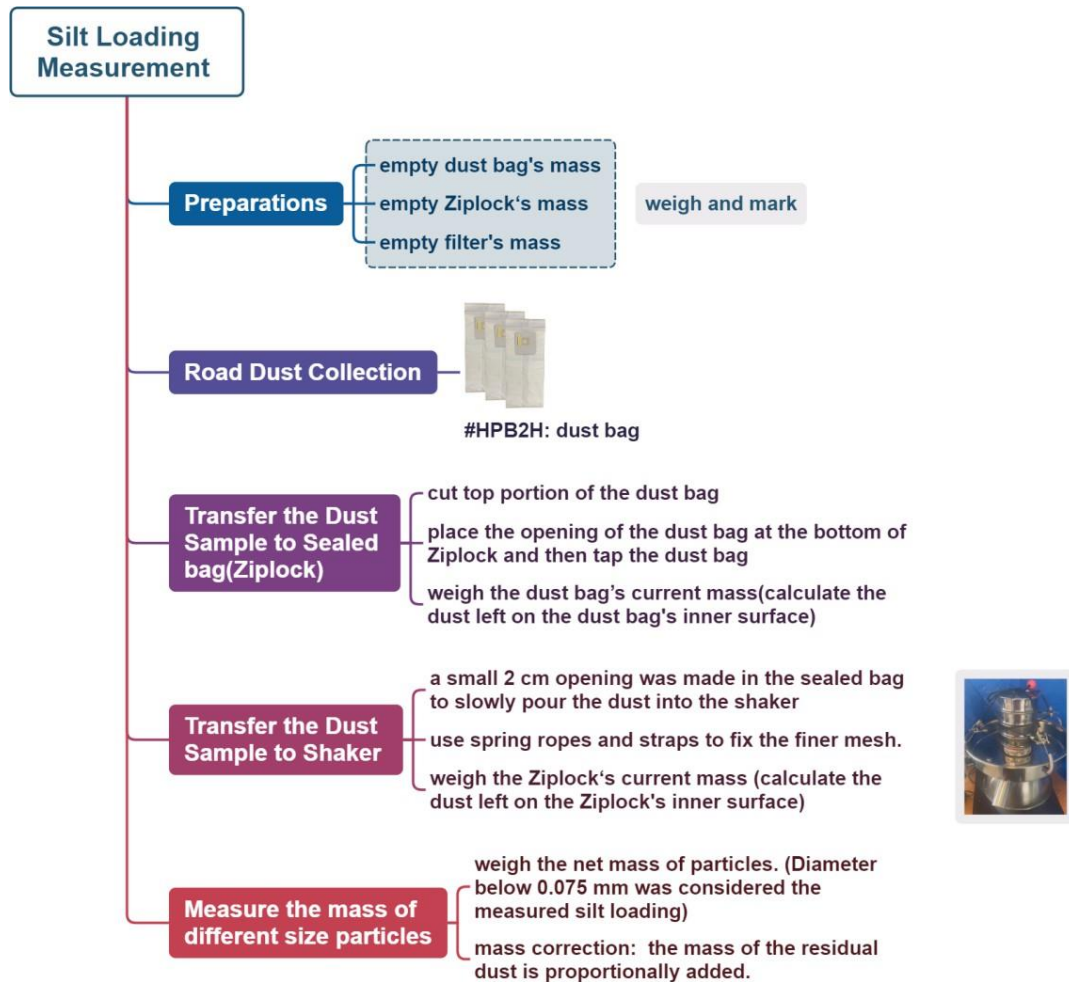


Figure 2.8 Silt Loading Measurement Process.

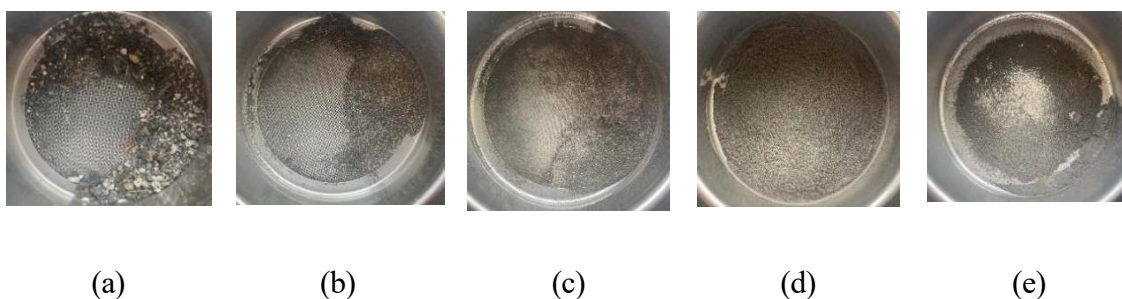


Figure 2.9 (a) Particles bigger than 0.315 mm. (b) Particles between 0.315 mm and 0.15 mm. (c) Particles between 0.15 mm and 0.075 mm. (d) Particles between 0.075 mm and 0.0385 mm. (e) Particles smaller than 0.0385 mm.

2.4 Improvements Made to Equipment During Field Studies

Following the initial field studies in spring 2023, challenges included balancing brush attachment tightness and manually controlling the UPS switch for the vacuum cleaner.

The following enhancements were implemented:

1. A new fixture allowed controlled upward and downward brush movement via a hollow tube connected to a spring-loaded part. This design ensured consistent contact between the brush and the ground (see [Figure 2.10](#)).
2. The UPS power source was relocated inside the van, enabling researchers to activate and deactivate the vacuum cleaner from within the mobile lab. This reduced errors and improved efficiency.
3. A Cen-Tec Systems 34839 vacuum brush was modified by removing rear bristles to prevent dust blockage and ensure effective collection. The contact area between the brush and ground was adjusted to account for bristle compression, increasing the collection area to 11 cm.
4. An automatic sieving system simulated manual shaking to sift dust samples through meshes of 0.315 mm, 0.15 mm, 0.075 mm, and 0.0385 mm. Finer mesh attachments were added to improve accuracy. Dust samples were weighed before and after sieving to calculate silt loading (dust mass per unit area).

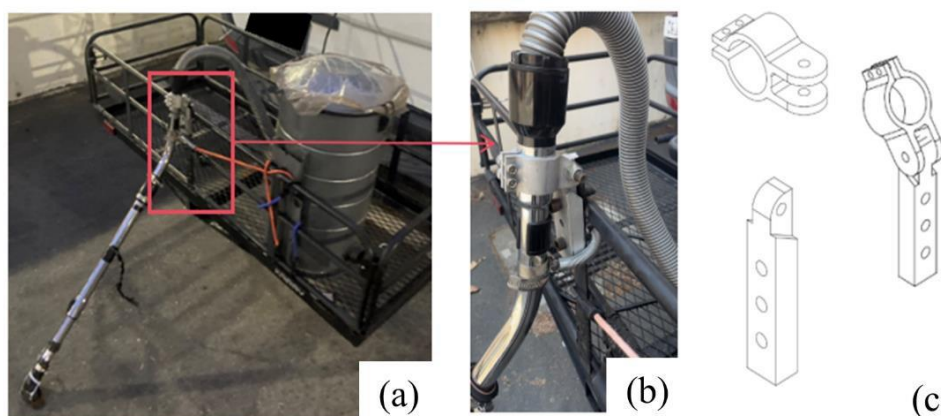


Figure 2.10 (a) Brush and tube attached to trailer (b) Details of attachment, (c) Components of attachment

The equipment list for the modified mobile platform is detailed in [Table 2.2](#).

Table 2.2 *Equipment list for mobile platforms.*

Number	Name	Type	Purpose
1	UPS generator	3.5 kW	Power the vacuum cleaner.
2	Vacuum cleaner	VacuMaid GV30	Collect road dust.
3	Brush Fixture	Machined parts	Adjust brush.
4	Trailer	60" x 24" x 14.4"	Hold the vacuum cleaner.
5	Brush	Cen-Tec Systems 34839 Vacuum Attachment, 5 x 2.5 x 4.5 inches	Sweep and vacuum dust from the roads
6	2D-sonic Anemometer	METSENS500 Campbell Scientific	Measure meteorological variables
7	Thermistor	IMET-XQ2	Measure temperature fluctuations
8	PurpleAir Flex sensor	3.5 in x 3.5 in x 5 in	Measure PM concentrations
9	Picarro	G2401-m	Measure CO/CO ₂ gas concentrations

2.5 Traffic Flow Measurements

Traffic data during road sampling included traffic speed, traffic flow, and the average vehicle weight on the road. The average vehicle weight was derived from the truck ratio, assuming an average truck weight of 16.5 tons and a passenger car weight of 1.95 tons.

The traffic data for the freeways were obtained from the Caltrans Performance Measurement System (PeMS). This information is collected in real-time from Loop

Detector Stations (LDS) embedded within the road surface, providing the traffic information for all lanes, updated every 5 minutes at a minimum (Caltrans 2020).

Traffic data for Chicago Ave. and Iowa Ave. was obtained with video equipment set up at intersections. Analysis of the video records provided information on the number of cars and trucks passing each camera, which was then converted to traffic flow and average vehicle weight on these roads. Vehicle speed was determined by using online tracker software (shown in Figure 2.11) that analyzes object motion speed from videos. The methodology involved setting up an XY coordinate system within the video frame, assuming a standard vehicle's length of 5 meters. Using a fixed point on each vehicle (e.g., door handle) as a reference, the new positions of this point were marked across video frames to determine the vehicle's speed. For each road, five vehicles were analyzed, and the average speed was used as the traffic speed for that particular experiment.

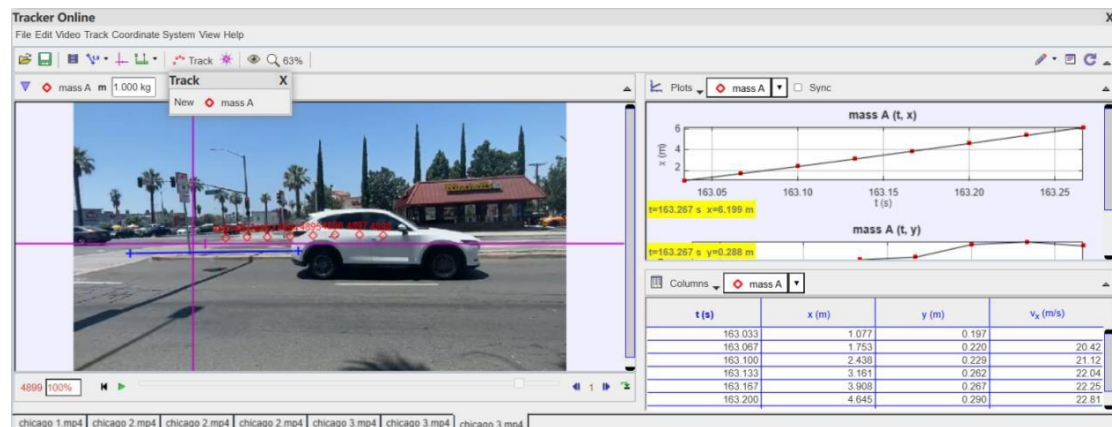


Figure 2.11 Diagram of the Tracker Interface and Operation.

2.6 Field Studies

The locations where the field studies were conducted are shown in Figure 1.3. Particulate concentration measurements were measured while the vehicle was in motion on the upwind and downwind sides of the road, followed by a stationary measurement for 10-15 minutes. To avoid errors associated with the precision of the PurpleAir instruments, we used the same sensor for both upwind and downwind sampling. The

sampling scenarios are shown in [Figure 1.4](#). Scenario 1 and 4 involved measurements taken while the vehicle was in motion on the downwind and upwind side of the road. In Scenario 2, we conducted turbulence measurements while the vehicle was parked on the downwind side of the road. This stationary setup allowed us to collect turbulence parameters, such as the standard deviation of the vertical velocity σ_w and surface heat flux Q_o . Scenario 3 includes stationary measurements taken upwind, aiding in the determination of background concentrations and relevant meteorological variables such as wind direction and speed.

A summary of sampling conducted in Spring 2024 is shown in

[Table 2.3](#).

Table 2.3 Summary of sampling information on roads.

Road Location	Sampling Duration [minutes]	Road Width [m]	Mean Silt Loading [g/m ²]	Mean Speed [mph]	Mean Vehicle Weight [tons]	Mean Traffic Flow [Veh/hour]
CA-55 Freeway	~4	50	0.031±0.015	68±1	2.83	12899
CA-60 Freeway	~4	30	0.019±0.015	51±15	2.06	7893
CA-71 Freeway	~4	49	0.053±0.005	61±5	2.23	6340
CA-91 Freeway	~7	30	0.024±0.007	58±11	2.05	7654
I-15 Freeway	~3	48	0.010±0.007	63±2	2.46	7465

Road Location	Sampling Duration [minutes]	Road Width [m]	Mean Silt Loading [g/m ²]	Mean Speed [mph]	Mean Vehicle Weight [tons]	Mean Traffic Flow [Veh/hour]
I-215 Freeway	~ 7	48	0.038±0.002	55±3	3.64	10254
Chicago Avenue	~ 5	24	0.221±0.060	42±10	3.20	2352
Iowa Avenue	~ 5	24	0.137±0.058	40±5	4.25	1875

This project involved conducting field studies at eight roadway sites. The on-road studies were carried out during the summer of 2023 and the spring of 2024 along sections of CA-91, CA-60, CA-71, CA-55, I-15, and I-215 freeways, as well as Chicago Avenue and Iowa Avenue in three counties in California.

Each field study lasted 3-5 hours at various roadway sections and times, providing primary samples for analysis.

2.7 Evaluation of Emission Factor Estimates

PurpleAir monitors have seldom been used on mobile platforms in previous studies, likely due to potential challenges in maintaining data quality, and the possible influence of vehicle motion on measurements. To evaluate the performance of mobile measurements, we compared the results from the stationary and vehicular monitors placed in the vicinity of the I-215 freeway. The mobile setup involved placing two monitors on each side of the van's doors, while the stationary setup included one monitor positioned on the downwind shoulder of the freeway and another approximately 100 meters upwind from the freeway. During the study, the van traveled back and forth along the freeway, collecting on-road PM data for around 2-5 minutes based on changing traffic situations. At the end of each loop, the van stopped for 5

minutes at both the downwind shoulder and the off-road upwind location to record PM and meteorological data. The differences in PM concentrations across the road were derived from the averages of the on-road downwind and off-road upwind measurements while the van was parked. Similarly, the difference in stationary PM concentrations was obtained from the down-wind shoulder measurements and the upwind stationary monitor during the vehicle's travel. Both PM concentration and meteorological data were used as inputs to the dispersion model to determine emission factors.

The comparison of emission factors obtained from these two monitor configurations at the Chicago street located in Riverside, shown in [Figure 2.12](#), suggests that concentration measurements from the mobile platform are adequate substitutes for stationary measurements: the coefficient of determination, R^2 , between PM_{10} and $PM_{2.5}$ emission factors measured by mobile and stationary PurpleAir units are 0.93 and 0.87, respectively, with little scatter between the two estimates.

The close comparison between estimates of emission factors from the dispersion model and the line source model also provides support for deriving emission factors from concentration measurements made on a moving platform.

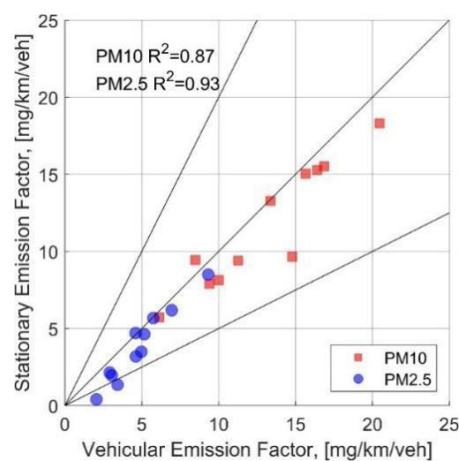


Figure 2.12 Emission factors estimated with mobile platforms compared to those using data from stationary monitors.

2.8 Results

2.8.1 Concentration of PM_{2.5}, PM₁₀, and CO₂

Measurements of PM_{2.5} and PM₁₀ concentrations were made along upwind and downwind sections of roadways. Each upwind-downwind loop lasted approximately 10 minutes, resulting in concentrations averaging over approximately two minutes corresponding to the time between the entry into and exit from the road of the mobile platform. Information on these measurements is presented in [Table 2.4](#) and [Table 2.5](#).

Table 2.4 Concentrations of PM_{2.5} and PM₁₀.

Road Name	Date	Time (PDT)	Downwind PM10 [ug/m ³]	Downwind PM2.5 [ug/m ³]	Upwind PM10 [ug/m ³]	Upwind PM2.5 [ug/m ³]	Delta PM2.5 [ug/m ³]	Delta PM10 [ug/m ³]
I-15	2024/04/21	13:31:15-13:47:12	5.19	3.51	4.53	2.97	0.54	0.66
	2024/05/05	17:03:48-17:11:49	4.86	3.51	4.53	3.37	0.14	0.33
	2024/07/23	17:07:05-17:15:25	19.48	14.29	14.83	11.81	2.48	4.65
	2024/07/23	17:23:30-17:31:41	19.79	15.12	15.04	12.05	3.07	4.75
	2024/07/23	17:40:57-17:48:57	16.73	12.45	14.64	11.42	1.03	2.09

Road Name	Date	Time (PDT)	Downwind PM10 [ug/m ³]	Downwind PM2.5 [ug/m ³]	Upwind PM10 [ug/m ³]	Upwind PM2.5 [ug/m ³]	Delta PM2.5 [ug/m ³]	Delta PM10 [ug/m ³]
I-215	2024/04/19	9:52:40-10:00:48	73.76	55.4	54.72	42.56	12.84	19.04
	2024/06/05	16:26:25-16:36:29	24.3	20.34	21.86	20.09	0.25	2.44
	2024/07/25	13:41:06-13:48:27	24.8	15.66	21.26	14.94	0.72	3.54
	2024/07/25	13:57:33-14:04:51	19.02	12.55	16.68	12	0.55	2.34
	2024/07/25	14:13:55-14:20:08	16.85	12.76	14.62	10.84	1.92	2.23
	2024/08/16	13:09:48-13:16:30	10.53	7.90	9.81	7.67	0.23	0.72
CA-55	2024/05/05	13:25:54-13:34:00	6.79	3.74	3.29	2.70	1.04	3.50
	2024/05/05	13:37:36-13:45:37	5.92	3.59	3.84	2.59	1.00	2.08
	2024/05/05	15:17:58-15:17:45	6.71	4.45	5.05	3.45	1.00	1.66
	2024/07/23	13:00:07-13:09:39	15.29	9.56	12.33	8.05	1.51	2.96
	2024/07/23	13:19:26-13:30:50	13.82	10.33	12.07	9.52	0.81	1.75
	2024/07/23	13:37:49-13:47:47	16.54	10.64	12.18	9.86	0.78	4.36

Road Name	Date	Time (PDT)	Downwind PM10 [ug/m ³]	Downwind PM2.5 [ug/m ³]	Upwind PM10 [ug/m ³]	Upwind PM2.5 [ug/m ³]	Delta PM2.5 [ug/m ³]	Delta PM10 [ug/m ³]
CA-60	2024/04/20	19:38:10-20:01:07	33.24	24.71	26.00	21.72	2.99	7.24
	2024/06/05	16:46:57-16:52:27	22.19	18.72	21.09	18.22	0.50	1.10
	2024/07/30	14:41:18-15:02:50	15.56	12.67	14.55	12.34	0.33	1.01
	2024/07/30	15:39:38-15:56:41	11.80	9.56	10.83	9.46	0.10	0.97
	2024/07/30	16:19:27-16:35:29	14.68	9.91	12.00	9.60	0.31	2.68
	2024/08/16	14:17:30-14:31:55	11.19	8.53	9.76	7.96	0.56	1.42
CA-71	2024/05/05	16:14:28-16:26:05	6.83	4.81	4.15	3.58	1.23	2.68
	2024/07/23	15:43:32-15:48:17	19.10	14.16	18.07	13.30	0.86	1.03
	2024/07/23	15:55:09-16:01:06	16.44	13.58	15.04	12.77	0.81	1.40
	2024/07/23	16:11:19-16:16:28	21.05	14.72	17.22	12.89	1.83	3.83

Road Name	Date	Time (PDT)	Downwind PM10 [ug/m ³]	Downwind PM2.5 [ug/m ³]	Upwind PM10 [ug/m ³]	Upwind PM2.5 [ug/m ³]	Delta PM2.5 [ug/m ³]	Delta PM10 [ug/m ³]
CA-91	2024/04/20	20:14:20-20:25:50	35.98	27.41	29.76	26.63	0.78	6.22
	2024/06/05	16:59:35-17:07:26	19.00	16.14	15.96	15.02	1.12	3.04
	2024/07/25	15:52:29-16:03:05	14.02	10.44	12.37	9.65	0.79	1.65
	2024/07/25	16:11:26-16:21:04	15.35	11.17	12.46	9.37	1.80	2.89
	2024/07/25	16:28:08-16:36:25	14.37	10.47	10.47	8.05	2.42	3.90
	2024/08/17	11:06:16-11:19:20	33.67	26.04	24.66	18.78	7.26	9.01
Iowa	2024/05/10	12:01:40-12:06:15	67.98	50.82	58.41	48.74	2.08	9.57
	2024/06/05	14:50:01-14:54:00	29.32	19.02	21.75	17.19	1.83	7.57
	2024/07/22	12:53:44-12:57:33	18.17	13.46	16.29	13.24	0.22	1.88
	2024/07/22	13:02:35-13:06:58	19.45	14.61	18.20	14.50	0.11	1.25
	2024/07/22	13:12:36-13:16:18	14.22	11.14	13.70	10.82	0.32	0.52

Road Name	Date	Time (PDT)	Downwind PM10 [ug/m ³]	Downwind PM2.5 [ug/m ³]	Upwind PM10 [ug/m ³]	Upwind PM2.5 [ug/m ³]	Delta PM2.5 [ug/m ³]	Delta PM10 [ug/m ³]
Chicago	2024/05/10	09:52:40-10:00:45	56.67	44.52	49.17	38.15	6.37	7.50
	2024/05/10	10:29:26-10:36:06	49.28	39.44	38.19	30.23	9.21	11.09
	2024/07/22	11:00:50-11:07:44	33.26	26.86	27.21	25.16	1.7	6.05
	2024/07/22	11:13:36-11:19:19	14.73	11.02	13.49	10.49	0.53	1.24
	2024/07/22	12:40:14-12:47:29	14.45	10.84	12.7	10.68	0.16	1.75
	2024/08/17	09:46:30-09:48:47	17.08	13.03	16.63	12.97	0.06	0.45

Table 2.5 Concentration of CO₂.

Road Name	Date	Time (PDT)	CO ₂ downwind ppm	CO ₂ upwind ppm	delta CO ₂ ppm
I-15	2024/04/21	13:31:15-13:47:12	453	370	83
I-215	2024/04/19	9:52:40-10:00:48	514	469	45
CA-55	2024/05/05	13:25:54-13:34:00	496	452	44
CA-60	2024/04/20	19:38:10-20:01:07	455	400	55
	2024/06/05	16:46:57-16:52:27	489	427	62
CA-71	2024/05/05	06:14:28-16:26:05	499	420	79
CA-91	2024/04/20	20:14:20-20:25:50	500	440	60
	2024/06/05	16:59:35-17:07:26	506	475	31

Road Name	Date	Time (PDT)	CO ₂ downwind ppm	CO ₂ upwind ppm	delta CO ₂ ppm
Iowa	2024/05/10	12:01:40-12:06:15	518	429	89
Chicago	2024/05/10	09:52:40-10:00:45	506	421	85

2.8.2 Meteorological Data

Table 2.6 presents the average wind speed (WS), wind direction (WD) and temperature (T) from different roads. Temperatures varied from 13.8°C to a maximum of about 39°C during the study periods. West winds dominated the study days with wind directions within 270 ± 45 degrees most of the time. Wind speed varied a lot due to the different seasons.

Table 2.6 Meteorological data.

Road Name	Date	Time (PDT)	Wind Speed m/s	Wind Direction degree	Temperature °C
I-15	2024/04/21	13:31:15-13:47:12	1.01	203.53	23.3
	2024/05/05	17:03:48-17:11:49	3.74	250.00	22.5
	2024/07/23	17:07:05-17:15:25	4.81	186.48	36.1
	2024/07/23	17:23:30-17:31:41	4.03	188.82	35.5
	2024/07/23	17:40:57-17:48:57	4.64	217.59	35

Road Name	Date	Time (PDT)	Wind Speed m/s	Wind Direction degree	Temperature °C
I-215	2024/04/19	9:52:40-10:00:48	2.30	234.23	13.8
	2024/06/05	16:26:25-16:36:29	2.02	275.00	29.4
	2024/07/25	13:41:06-13:48:27	0.80	251.91	37.7
	2024/07/25	13:57:33-14:04:51	2.05	240.36	38
	2024/07/25	14:13:55-14:20:08	1.70	233.77	38.3
	2024/08/16	13:09:48-13:16:30	0.82	214.48	33.8
CA-55	2024/05/05	13:25:54-13:34:00	1.34	253.33	18.3
	2024/05/05	13:37:36-13:45:37	1.21	264.00	18.6
	2024/05/05	15:17:58-15:17:45	2.65	215.00	18.8
	2024/07/23	13:00:07-13:09:39	2.00	228.83	36.6
	2024/07/23	13:19:26-13:30:50	3.28	305.19	36.9
	2024/07/23	13:37:49-13:47:47	2.60	217.29	37.2
CA-60	2024/04/20	19:38:10-20:01:07	1.60	240	21.1
	2024/06/05	16:46:57-16:52:27	2.53	293.33	29.4
	2024/07/30	14:41:18-15:02:50	2.35	161.89	34.4
	2024/07/30	15:39:38-15:56:41	0.87	291.30	33.8
	2024/07/30	16:19:27-16:35:29	1.15	245.05	33.3
	2024/08/16	14:17:30-14:31:55	1.55	228.91	35.8
CA-71	2024/05/05	16:14:28-16:26:05	1.01	262.50	18.8
	2024/07/23	15:43:32-15:48:17	1.58	206.17	37.2
	2024/07/23	15:55:09-16:01:06	3.24	227.59	36.1
	2024/07/23	16:11:19-16:16:28	2.58	312.05	35

Road Name	Date	Time (PDT)	Wind Speed m/s	Wind Direction degree	Temperature °C
CA-91	2024/04/20	20:14:20-20:25:50	1.59	271.42	16.1
	2024/06/05	16:59:35-17:07:26	2.27	295	29.4
	2024/07/25	15:52:29-16:03:05	3.44	237.81	38.3
	2024/07/25	16:11:26-16:21:04	2.47	329.40	38.3
	2024/07/25	16:28:08-16:36:25	2.81	318.673	38.3
	2024/08/17	11:06:16-11:19:20	1.55	91.10	25.5
Iowa	2024/05/10	12:01:40-12:06:15	3.03	230.48	26.1
	2024/06/05	14:50:01-14:54:00	3.03	230.48	31.6
	2024/07/22	12:53:44-12:57:33	3.98	283.15	36.1
	2024/07/22	13:02:35-13:06:58	2.75	234.44	36.6
	2024/07/22	13:12:36-13:16:18	2.00	277.64	37.2
Chicago	2024/05/10	09:52:40-10:00:45	0.65	74.62	22.7
	2024/05/10	10:29:26-10:36:06	3.03	230.48	27.2
	2024/07/22	11:00:50-11:07:44	3.54	209.47	32.2
	2024/07/22	11:13:36-11:19:19	1.86	241.69	33.6
	2024/07/22	12:40:14-12:47:29	2.08	182.90	36.1
	2024/08/17	09:46:30-09:48:47	3.31	205.35	22.7

2.8.3 Traffic Count and Traffic Speed

Table 2.7 and **Table 2.8** presents data on traffic flow, speed, truck ratio, and average vehicle weight for various road types. Traffic flow values reflect the combined volume of vehicles traveling in both directions, while traffic speed and truck ratio represent values averaged over both directions. The average vehicle weight was estimated based on the truck ratio.

As shown in **Table 2.7** and **Table 2.8**, traffic flow on highways ranges from approximately 5,000 to 10,000 vehicles per hour, with average speeds between 38 and 70 mph. The truck ratio on highways varies significantly, influenced by both the highway type and time of day. In contrast, traffic flow on city roads is around 1,000 to 3,000 vehicles per hour, with speeds ranging from 16 to 40 mph, also depending on the time of day. Generally, the truck ratio on city roads is higher than on highways.

Table 2.7 Traffic conditions on different roads in 2023.

Road Name	Time	Traffic flow veh/hour	Traffic speed mph	Truck ratio %	Average weight Tons
I-215	2023 May	5364	50.24	4.47%	2.60
		6468	45.93	4.64%	2.62
		5880	41.74	4.08%	2.54
		6120	46.25	4.31%	2.58
		5616	53.69	4.49%	2.60
		5664	56.73	4.66%	2.63
		5940	56.14	4.85%	2.66
		5376	47.89	4.24%	2.57
		4536	39.46	2.91%	2.37
		6468	44.66	4.27%	2.57
		6072	44.00	3.95%	2.53
		6252	53.28	4.03%	2.54
		5112	61.56	4.23%	2.56
		5052	57.40	3.80%	2.50
		5400	47.65	3.56%	2.47
		5352	42.46	2.91%	2.37
		5088	44.61	3.30%	2.43
		5736	43.18	3.35%	2.44
		6264	41.60	3.64%	2.48
		6792	39.82	4.24%	2.57
5844	37.92	4.11%	2.55		

Road Name	Time	Traffic flow veh/hour	Traffic speed mph	Truck ratio %	Average weight Tons
CA-91	2023 May	9940	59.74	2.45%	2.31
		8944	62.50	2.64%	2.33
		8648	63.16	2.78%	2.35
		9048	52.50	2.12%	2.26
		7552	62.52	2.91%	2.37
		9916	57.95	2.22%	2.27
		10280	57.74	2.18%	2.27
		6876	64.08	3.08%	2.40
		6436	60.48	2.73%	2.35
		9620	56.14	2.20%	2.27
		9488	51.24	1.73%	2.20
		10428	55.95	2.07%	2.25

Road Name	Time	Traffic flow veh/hour	Traffic speed mph	Truck ratio %	Average weight Tons
Chicago	2023 May	2512	27.10	17.49%	4.49
		2338	28.62	14.37%	4.04
		1460	36.26	17.44%	4.49
		1071	39.64	13.82%	3.96
		1936	32.11	22.76%	5.26
		1716	34.03	26.30%	5.78
		1903	32.40	20.28%	4.90
		2047	31.14	17.34%	4.47
		2162	30.15	15.04%	4.14
		1372	37.02	12.35%	3.75
		1707	34.11	19.78%	4.83
		1573	35.27	18.01%	4.57
		2282	29.10	17.90%	4.55
		1760	33.64	15.44%	4.20
		1919	32.26	17.51%	4.50

Road Name	Time	Traffic flow veh/hour	Traffic speed mph	Truck ratio %	Average weight Tons
Iowa	2023 May	1883	32.58	24.65%	5.54
		2150	30.25	21.82%	5.13
		1819	33.13	24.12%	5.46
		2367	28.37	21.00%	5.01
		1426	36.55	17.61%	4.51
		1572	35.28	27.79%	5.99
		1563	35.35	30.06%	6.32
		1556	35.42	17.80%	4.54
		2238	29.48	28.70%	6.13
		2077	30.88	21.97%	5.15
		2932	23.44	12.47%	3.76
		2241	29.46	14.53%	4.06
		1904	32.39	16.64%	4.37
		1885	32.56	27.67%	5.98
		2184	29.96	25.61%	5.68
		2127	30.45	24.20%	5.47
		2205	29.78	20.58%	4.94

Table 2.8 Traffic conditions on different roads in 2024.

Road Name	Date	Time (PDT)	Traffic flow veh/hour	Traffic speed Mph	Truck ratio %	Average weight tons
I-15	2024/04/21	13:31:15-13:47:12	8095	61.65	6.00%	2.82
	2024/05/05	17:03:48-17:11:49	6834	64.7	8.90%	3.24
	2024/07/23	17:07:05-17:15:25	8784	60.5	6.30%	2.87
	2024/07/23	17:23:30-17:31:41	8412	58.75	7.05%	2.96
	2024/07/23	17:40:57-17:48:57	8232	61.1	6.95%	2.96
I-215	2024/04/19	9:52:40-10:00:48	10974	52.37	12.00%	3.70
	2024/06/05	16:26:25-16:36:29	9534	57.1	17.40%	4.48
	2024/07/25	13:41:06-13:48:27	9468	45.1	12.50%	3.77
	2024/07/25	13:57:33-14:04:51	10176	45.15	13.35%	3.89
	2024/07/25	14:13:55-14:20:08	10092	45.4	13.75%	3.95
	2024/08/16	13:09:48-13:16:30	10464	48.95	10.90%	3.53
CA-55	2024/05/05	13:25:54-13:34:00	14517	67.25	5.00%	2.68
	2024/05/05	13:37:36-13:45:37	12346	67.15	12.40%	3.75
	2024/05/05	15:17:58-15:17:45	11834	68.15	11.80%	3.67
	2024/07/23	13:00:07-13:09:39	10560	61.25	4.85%	2.66
	2024/07/23	13:19:26-13:30:50	11508	60.5	5.70%	2.78
	2024/07/23	13:37:49-13:47:47	11472	62.05	3.70%	2.49

Road Name	Date	Time (PDT)	Traffic flow veh/hour	Traffic speed Mph	Truck ratio %	Average weight tons
CA-60	2024/04/20	19:38:10-20:01:07	7642	62.3	5.00%	2.68
	2024/06/05	16:46:57-16:52:27	8652	36.6	8.60%	3.20
	2024/07/30	14:41:18-15:02:50	7008	46.1	3.10%	2.40
	2024/07/30	15:39:38-15:56:41	7812	45.35	2.75%	2.35
	2024/07/30	16:19:27-16:35:29	7500	47.2	2.65%	2.34
	2024/08/16	14:17:30-14:31:55	7956	42.25	12.65%	3.79
CA-71	2024/05/05	16:14:28-16:26:05	6340	60.8	6.00%	2.82
	2024/07/23	15:43:32-15:48:17	6948	56.6	6.05%	2.83
	2024/07/23	15:55:09-16:01:06	6336	55.45	5.90%	2.81
	2024/07/23	16:11:19-16:16:28	6504	56.65	6.30%	2.87
CA-91	2024/04/20	20:14:20-20:25:50	7057	65.7	4.00%	2.53
	2024/06/05	16:59:35-17:07:26	8250	50.25	5.90%	2.81
	2024/07/25	15:52:29-16:03:05	8976	48.45	8.40%	3.17
	2024/07/25	16:11:26-16:21:04	9048	50	5.50%	2.75
	2024/07/25	16:28:08-16:36:25	9000	52.45	5.75%	2.79
	2024/08/17	11:06:16-11:19:20	7380	40.65	4.15%	2.55
Iowa	2024/05/10	12:01:40-12:06:15	2352	28.4936	13.00%	3.84
	2024/06/05	14:50:01-14:54:00	2181	29.9813	11.00%	3.55
	2024/07/22	12:53:44-12:57:33	1400	36.91	13.00%	3.84
	2024/07/22	13:02:35-13:06:58	1140	39.3	12.00%	3.70
	2024/07/22	13:12:36-13:16:18	1220	38.02	10.00%	3.41

Road Name	Date	Time (PDT)	Traffic flow veh/hour	Traffic speed Mph	Truck ratio %	Average weight tons
Chicago	2024/05/10	09:52:40-10:00:45	760	42.344	13.00%	3.84
	2024/05/10	10:29:26-10:36:06	2010	16.684	12.00%	3.70
	2024/07/22	11:00:50-11:07:44	1740	23.218	25.00%	5.59
	2024/07/22	11:13:36-11:19:19	1260	34.6	11.00%	3.55
	2024/07/22	12:40:14-12:47:29	1170	36.9	5.00%	2.68
	2024/08/17	09:46:30-09:48:47	1230	35.94	7.00%	2.97

2.8.4 Silt Loading

Table 2.9 below presents silt loading data obtained from the analysis of road dust samples in the study of 2024. The silt loading data shows distinct differences between highways and city roads. On highways (e.g., I-15, I-215, CA-55), silt loading values typically range from approximately 0.0012 to 0.0534 g/m², reflecting lower dust accumulation likely due to higher speeds. In contrast, city roads such as Iowa and Chicago exhibit higher silt loading values, ranging from about 0.0102 to 0.2640 g/m².

Table 2.9 Silt loading from different roads in 2024.

Road Name	Date	Distance Km	Silt loading g/m ²
I-15	2024/04/21	11.45	0.0156
	2024/05/05	5.73	0.0048
	2024/07/23	5.73	0.0031
	2024/07/23	5.73	0.0028
	2024/07/23	5.73	0.00228

Road Name	Date	Distance Km	Silt loading g/m ²
I-215	2024/04/19	8.04	0.03918
	2024/06/05	4.08	0.0363
	2024/07/25	4.08	0.0012
	2024/07/25	4.08	0.0017
	2024/07/25	4.08	0.00217
	2024/08/16	4.08	0.0266
CA-55	2024/05/05	9.39	0.0478
	2024/05/05	9.39	0.0286
	2024/05/05	4.7	0.0179
	2024/07/23	5.14	0.0172
	2024/07/23	5.14	0.0043
	2024/07/23	5.14	0.0085
CA-60	2024/04/20	12.87	0.0302
	2024/06/05	2.1	0.0084
	2024/07/30	6.82	0.0044
	2024/07/30	6.82	0.0082
	2024/07/30	6.82	0.0026
	2024/08/16	6.82	0.0085
CA-71	2024/05/05	5.15	0.0534
	2024/07/23	2.84	0.0118
	2024/07/23	2.84	0.0071
	2024/07/23	2.84	0.0136

Road Name	Date	Distance Km	Silt loading g/m ²
CA-91	2024/04/20	10.62	0.0181
	2024/06/05	4.6	0.0289
	2024/07/25	5.5	0.0102
	2024/07/25	5.5	0.0091
	2024/07/25	5.5	0.0115
	2024/08/17	5.5	0.0286
Iowa	2024/05/10	3.25	0.1787
	2024/06/05	3.25	0.2640
	2024/07/22	3.25	0.0391
	2024/07/22	3.25	0.0605
	2024/07/22	3.25	0.0652
Chicago	2024/05/10	3.25	0.1034
	2024/05/10	2.44	0.1781
	2024/07/22	1.03	0.0954
	2024/07/22	2.44	0.0244
	2024/07/22	2.44	0.0102
	2024/08/17	2.44	0.0211

3 Analysis of Components of Road Dust

3.1 Field Sampling

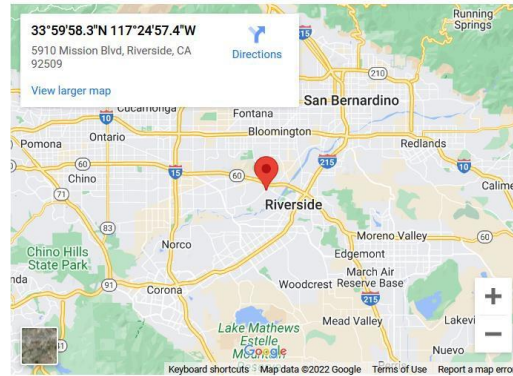
In Summer 2021, we planned a field study to test out using a mobile van for measuring on-road composition of submicron aerosols, including their non-refractory components and black carbon. It turned out the mobile van was not equipped to keep up with the power/cooling needed to operate the mass spectrometer. Given the additional power that would have been needed to operate an Xact-625i monitor for aerosol elemental composition as well as the longer averaging time the instrument needs to obtain enough mass for accurate XRF analysis, we concluded that mobile measurements using this van were not promising for the next set of field studies. Instead, we decided to use stationary measurements at some of the sites managed by the South Coast Air Quality Management District in Riverside County to obtain ambient measurements of PM₁₀ and PM_{2.5} concentrations and elemental composition needed for source apportionment. The chosen sites were a near-road site in Ontario (near Etiwanda Ave, [Figure 3.1 \(a\)](#)) and a suburban site in Rubidoux ([Figure 3.1 \(b\)](#))- both of which are located in eastern part of the Los Angeles Basin, and therefore are typically downwind of emissions from the western sections of the Basin. Carrying out measurements at these sites also provided us the opportunity to access data from other measurements available at the site from either the SCAQMD or by coPI Bahreini, thereby assisting with interpretation of the source apportionment results. [Table 3.1](#) summarizes the location, duration, and available measurements for each of the different phases of the stationary field projects.

Ontario - Near Road (Etiwanda)



(a)

Rubidoux - Mission Blvd



(b)

Figure 3.1 (a) location of the near-road sampling site in Ontario/Etiwanda; (b) location of the suburban sampling site in Rubidoux.

The Xact monitor was rented for the different phases of the project. When deployed at Ontario/Etiwanda, an inlet system was used with the intent of switching between sampling PM_{2.5} and PM₁₀ particles every hour, providing 12 measurements for each size fraction per day. At Rubidoux, the rented Xact instrument sampled PM₁₀ at an hourly rate while another instrument available through the NSF-funded ASCENT program (for which coPI Bahreini is a coPI) provided hourly PM_{2.5} measurements, therefore, doubling the number of data points available for each size fraction in a given day and providing a higher-time resolution on the compositional data. At Rubidoux, PM_{2.5} BC and non-refractory aerosol composition were also available through ASCENT, at high time-resolution (1 min for BC and 10 min for non-refractory components of PM_{2.5}, meaning organic aerosols, sulfate, nitrate, chloride (non-refractory), ammonium).

The eBAM instruments were borrowed from SCAQMD to provide hourly PM₁₀ and/or PM_{2.5} mass concentration.

Table 3.1 Summary of measurements for different phases of the project. ⁺ Data not available between Feb. 4-8, 2023. * Data suggests that the switching valve was not operating as designed.

Project Phase	Deployment Period	Measurements made by coPI Bahreini	Measurements available from SCAQMD
Phase 1 Ontario/ Etiwanda	Winter; Feb. 2023	PM ₁₀ and PM _{2.5} elemental (Xact, Jan 31- Feb. 16) PM ₁₀ and ⁺ PM _{2.5} mass concentration (eBAMs, Feb. 3-16)	NOx, BC, wind speed, wind direction
Phase 2 Ontario/ Etiwanda	Summer; Aug. 2023	*PM ₁₀ and PM _{2.5} elemental (Xact, Aug. 15- 25) PM ₁₀ mass concentration (eBAM, Aug. 18-25)	NOx, BC, wind speed, wind direction
Phase 3 Rubidoux	Summer; Aug.-Sep. 2023	PM ₁₀ elemental (Xact Aug. 25- Sep 5) PM _{2.5} elemental (Xact Aug 1- Sep 30) PM _{2.5} BC (AE33, Aug 1- Sep 30) PM _{2.5} non-refractory composition (ACSM, Aug 1- Sep 30)	CO, NOx, O ₃ , PM ₁₀ and PM _{2.5} mass, wind speed, wind direction

3.2 Instrument Calibrations and QA/QC

Upon receiving the rented Xact instruments, the instrument was calibrated using 5 elements (Cr, Ba, Zn, Pb, Cd). Results were found to be within 10% of the expected values. Furthermore, after installation, instrument flow rate was checked and the instrument was leak-checked. Additionally, everynight, the XRF energy levels were checked automatically using two internal standards (Cr and Nb) and the response to 4

internal standards (Cr, Nb, Cd, Pb) were rechecked. Figure 3.2 shows extremely high stability of the instrument response during phase 1. Similar behavior was observed during other deployments. Similar checks and calibrations are carried out routinely for the ASCENT instrument.

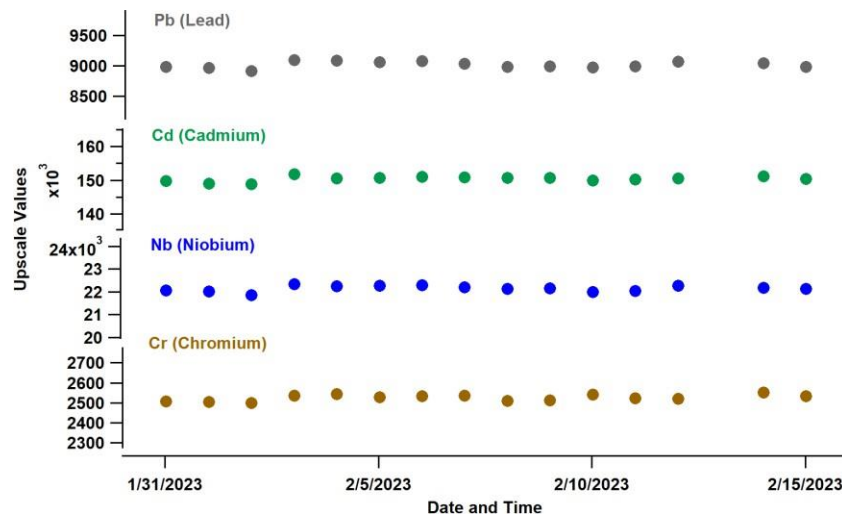


Figure 3.2 Example of the nightly calibration response of Xact-625i to internal standards.

Before receiving the eBAM instruments, SCAQMD staff had performed detail calibration of the instruments. Upon receiving the eBAM units, the flow rate and leak rate were checked again. During Phase 3 when eBAM-PM10 (borrowed from SCAQMD) was deployed at Rubidoux, we had a chance to compare its measurements to the colocated PM10 data provided directly by SCAQMD from their regular measurements using a BAM instrument at the site. As shown in Figure 3.3, the two data sets are highly correlated ($r^2=0.85$) and the agreement is reasonable to within 25%. This level of correlation and agreement gives us confidence about the reliability of eBAM-PM10 units deployed at Ontario/Etiwand during earlier phases of the project. We do not have an independent method to verify the performance of eBAM-PM2.5 instruments.

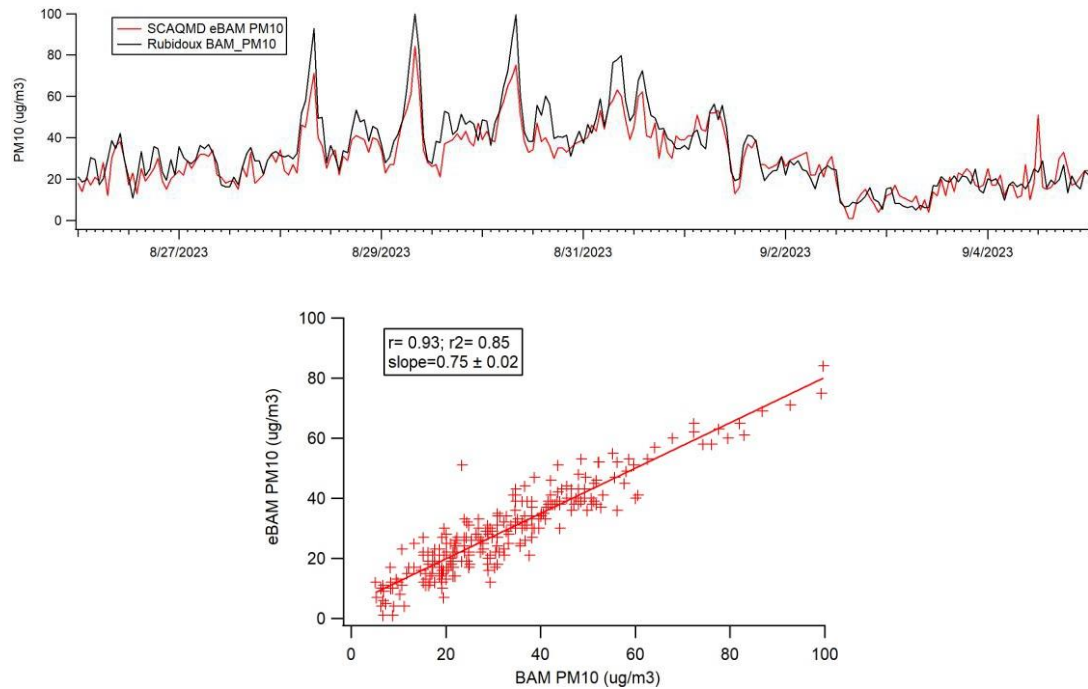


Figure 3.3 Comparison of borrowed eBAM-PM10 and SCAQMD-operated BAM-PM10 instruments at Rubidoux during Phase 3.

3.3 Results

3.3.1 Elemental Composition Measurements

The Xact monitor measured concentrations of several elements, with varying levels of certainty, namely, Al, Si, S, Cl, K, Ca, Ti, V, Cr, Mn, Fe, Ni, Cu, Zn, As, Br, Rb, Sr, Sn, Ba, Pt, and Bi. An estimate of the uncertainty, based on the influence of interfering elements to the XRF signal, are automatically provided for each sample. Following the guidelines from the manufacturer, in our analysis we focus on elements with signal values higher than the reported uncertainty. As an example, [Figure 3.4](#) shows the average concentration to uncertainty value of several of the elements (during Phase 1) that are important markers for different types of PM. As shown here for the PM10 fraction, As and Ni (tracers of anthropogenic/industrial processes) have the lowest concentration to uncertainty ratio, while main tracers of crustal material (Ca, Fe, Si, Mn, Ti, K), brake wear (Ba and Cu), and tire wear (Zn) have significantly higher ratios and are thus measured with much more certainty. The trends are similar for the PM2.5

fraction, with the exception of Cr, Si and Mn. These different confidence or uncertainty levels have been considered explicitly in our source apportionment efforts.

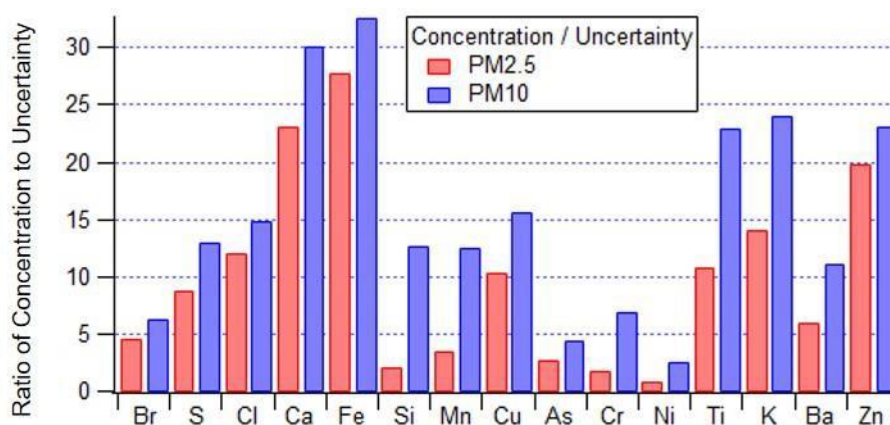


Figure 3.4 Distribution of the average concentration to uncertainty values reported for key elements in PM10 and PM2.5 during Phase 1.

3.3.2 Elemental Spatial Distribution

Phase 1- Winter Ontario/Etiwanda

During Phase 1, the Ontario/Etiwanda site was predominantly under the influence of southwesterly and northeasterly winds. These general daytime onshore flows and nighttime offshore flows are typical in S. California. However, during Phase 1, periods of more intense wind events associated with offshore, northeasterly Santa Ana winds were also encountered. During these events, it is likely that air masses sampled at the site had a higher influence of dust emissions from natural crustal sources upwind of the site consistent with a higher fraction of high-concentration crustal material observed in this wind sector (Figure 3.5 and Figure 3.6). However, as shown in Figure 3.7, vehicular and truck traffic-related emission tracers, namely BC, CO, and NO_x, were still enhanced under the influence of northeasterly winds, likely due to the reversal of the flow of air masses transported previously to the inland areas. Therefore, we did not limit our analysis to only southwesterly flows.

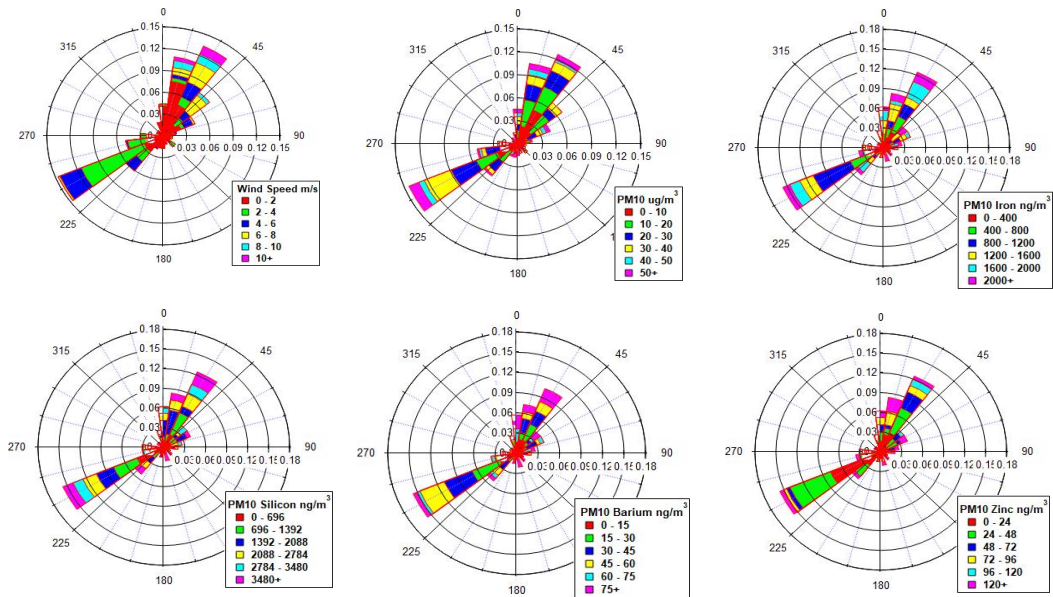


Figure 3.5 Wind roses of wind speed, PM10, and several trace elements of PM10 (Fe and Si as tracers of crustal material, Ba as brake wear, and Zn and tire wear) for Phase 1 (Ontario/Etiwanda in Winter 2023).

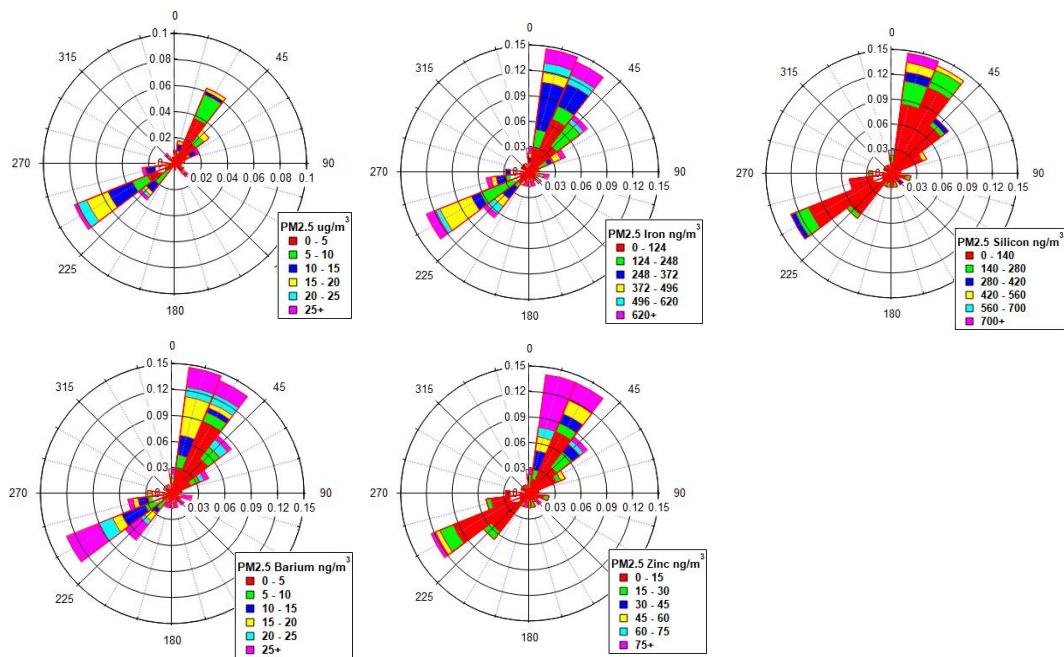


Figure 3.6 Wind roses of PM2.5 and several trace elements of PM2.5 (Fe and Si as tracers of crustal material, Ba as brake wear, and Zn as tire wear) for Phase 1 (Ontario/Etiwanda in Winter 2023).

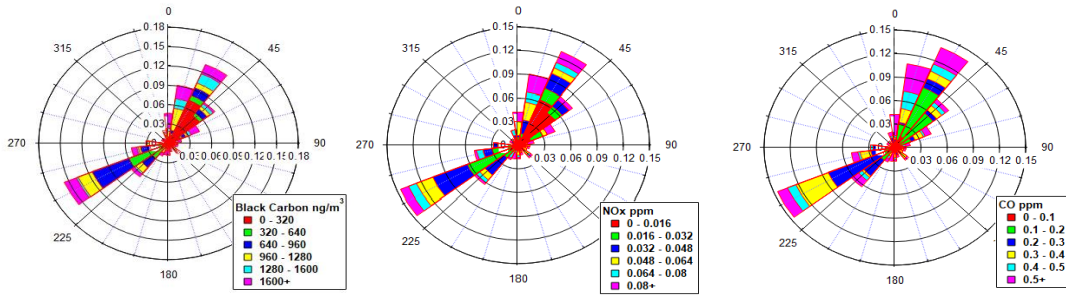


Figure 3.7 Wind rose of BC, NO_x, and CO as markers of traffic- related emissions for Phase 1 (Ontario/Etiwanda in Winter 2023).

Figure 3.8 compares the distribution of the key elements that are indicators of crustal material, brake wear, tire wear, or industrial activities between PM₁₀ and PM_{2.5}. For all of these elements, factors of ~2-10 more mass is found in PM₁₀, with crustal material being dominated in the PM₁₀ fraction.

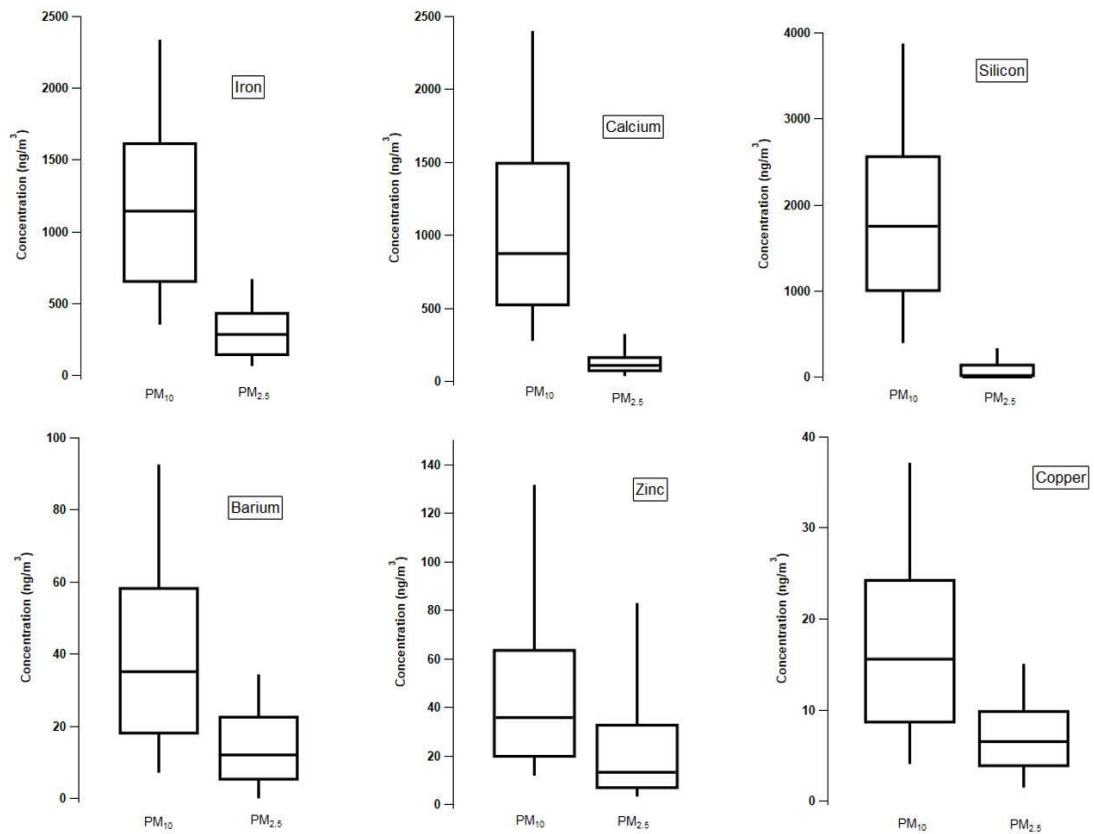


Figure 3.8 Box and whisker plots representing 10th, 25th, 50th, 75th, and 90th percentile values of PM₁₀ and PM_{2.5} mass concentrations of Fe, Ca, Si, Ba, Zn, and Cu during Phase 1 (Ontario/Etiwanda, Winter 2023).

Phase 2- Summer Ontario/ Etiwanda

During Phase 2, Xact was deployed at Ontario/Etiwanda near-road site with a switching inlet again along with an eBAM-PM10 instrument. As apparent in [Figure 3.9](#), the site was under the influence of southwesterly flows, and therefore, directly downwind of emissions from western sections of LA Basin.

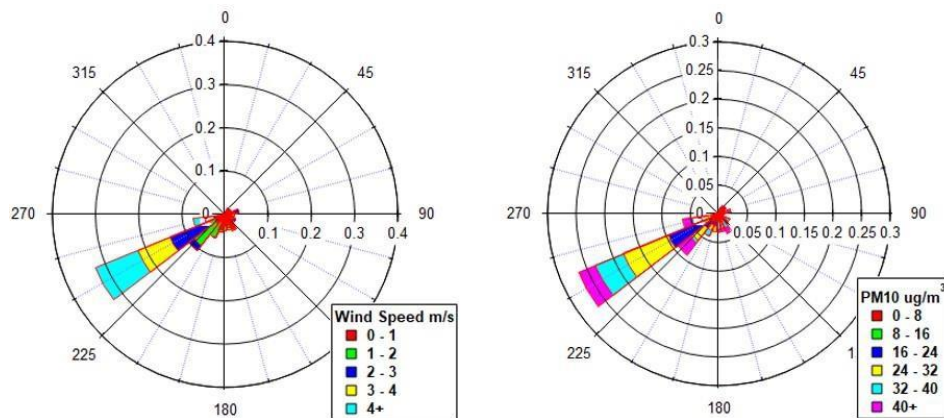


Figure 3.9 Wind roses of wind speed and PM10 for Phase 2 (Ontario/Etiwanda in Summer 2023).

However, careful look at the elemental data revealed that the inlet switching valve was likely not working as designed during this phase. Starting on Aug. 21st, the reported PM2.5 and PM10 concentrations of all the elements are almost exactly the same, indicating that the switching valve had completely failed. When examining the distribution of the key elements between PM2.5 and PM10 ([Figure 3.10](#)), the median values in PM2.5 are still lower than in PM10; however, the 75th and 90th percentile values are highly similar. This observation suggests that the valve was perhaps only partially switching during earlier times of deployment; therefore, there is cross contamination between sampling PM10 and PM2.5. As such the data from Phase 2 are not used in any further analysis.

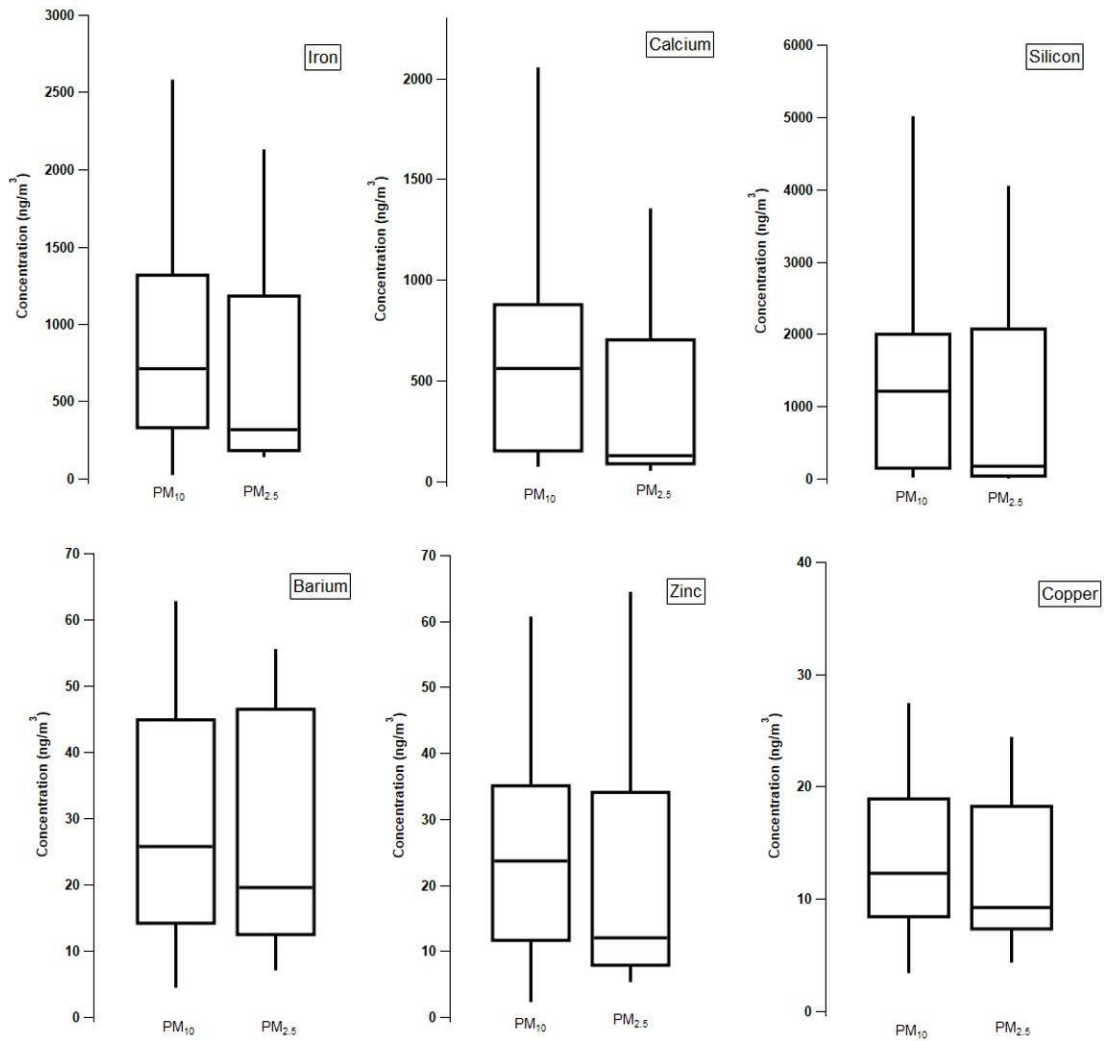


Figure 3.10 Box and whisker plots representing 10th, 25th, 50th, 75th, and 90th percentile values of PM_{10} and $\text{PM}_{2.5}$ mass concentrations of Fe, Ca, Si, Ba, Zn, and Cu during Phase 2 (Ontario/Etiwanda, Summer 2023). Data suggest the switching inlet valve was not working properly during this phase.

Phase 3- Summer Rubidoux

During the summertime deployment at Rubidoux, the site was predominantly under the influence of westerly flows at low to moderate wind speeds (Figure 3.11 and Figure 3.12). Enhancements in traffic related emissions, BC, NO_x, and CO, in westerly flows confirm persistent transport of emissions from western sections of the LA Basin to the site.

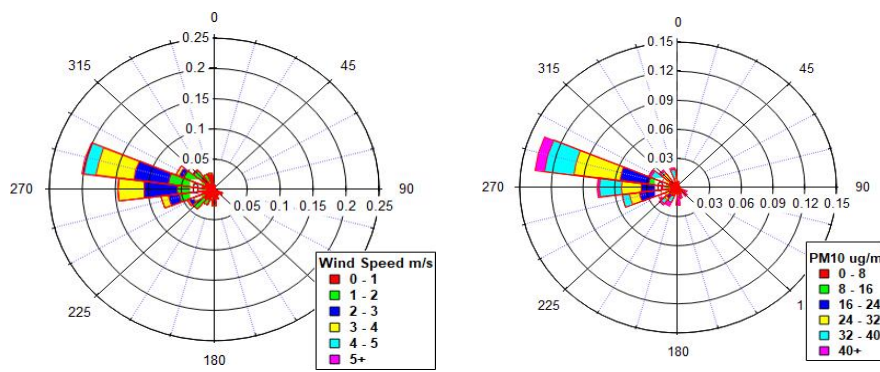


Figure 3.11 Wind rose of wind speed and PM10 for Phase 3 (Rubidoux in Summer 2023).

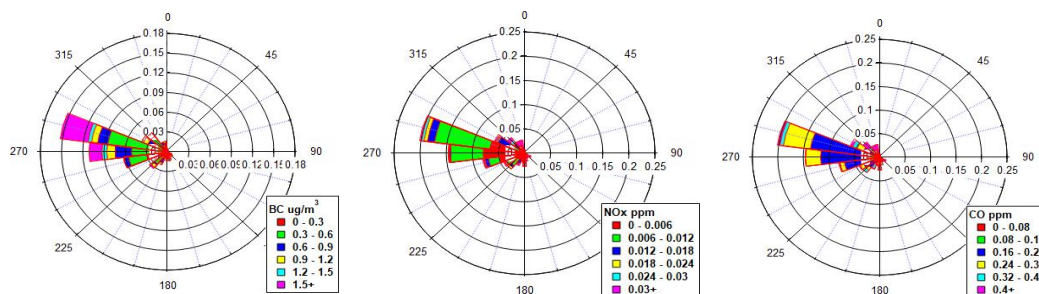


Figure 3.12 Wind rose of BC, NOx, and CO as markers of traffic-related emissions for Phase 3 (Rubidoux in Summer 2023).

Figure 3.13 demonstrates the distribution of the key elements among PM10 and PM2.5 during Phase 3. The results are consistent with earlier observations in Ontario/Etiwanda during Winter 2023, with much higher concentrations of each element being observed in PM10. These results confirm that Summer Ontario/Etiwanda elemental measurements are not valid and that the significant presence of these elements in PM10 is not due to influence of northerly/northeasterly winds observed during Phase 1.

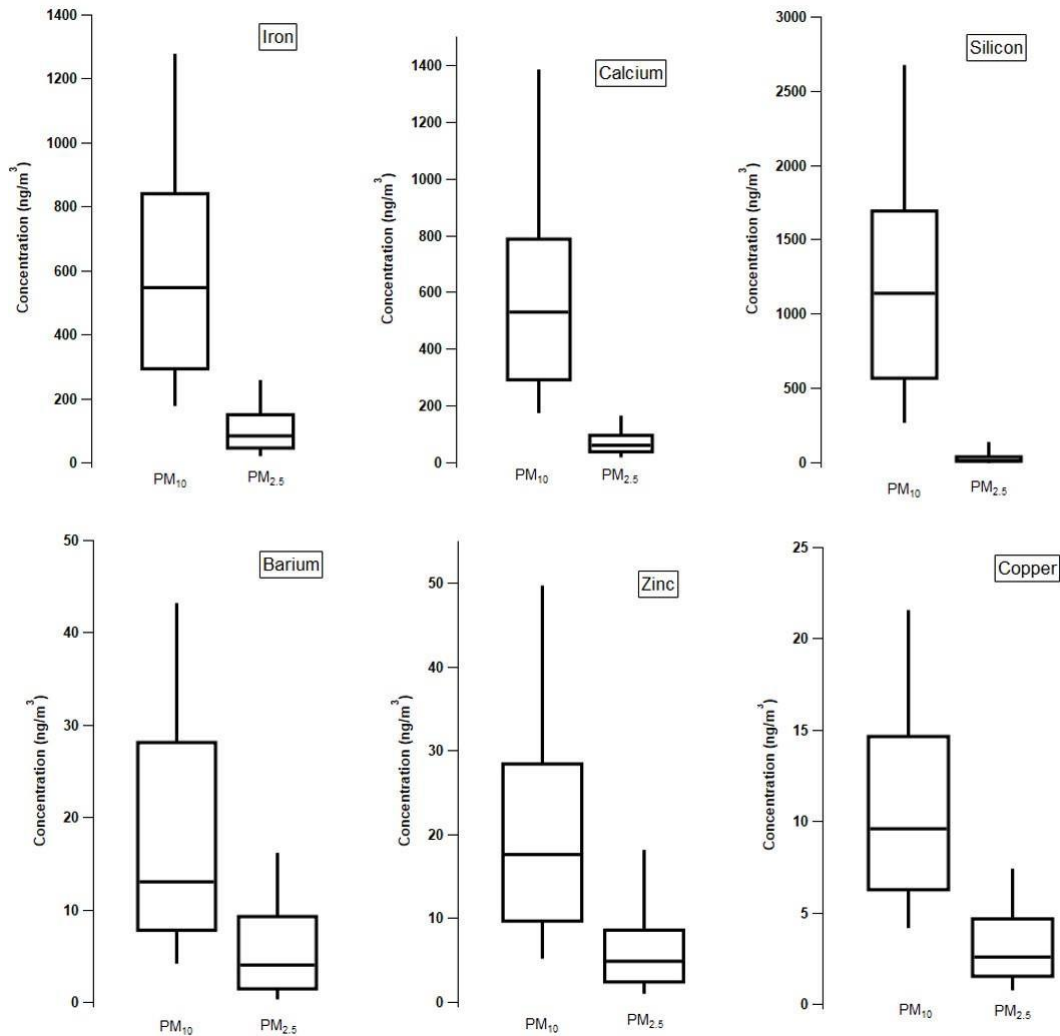


Figure 3.13 Box and whisker plots representing 10th, 25th, 50th, 75th, and 90th percentile values of PM_{10} and $\text{PM}_{2.5}$ mass concentrations of Fe, Ca, Si, Ba, Zn, and Cu during Phase 3 (Rubidoux in Summer 2023). $\text{PM}_{2.5}$ statistics are based on the data collected only during the deployment of Xact- PM_{10} for consistency in comparison.

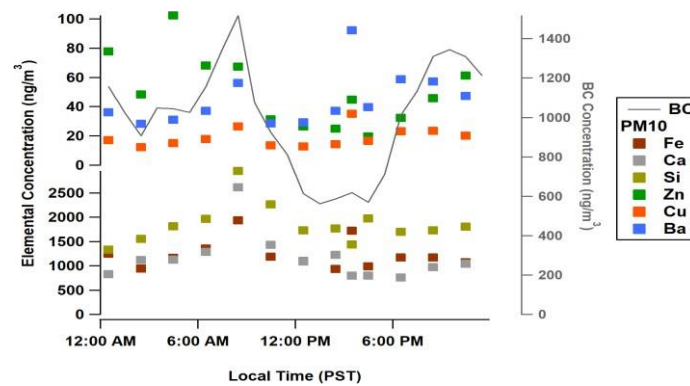
3.3.3 Diurnal Profiles

Phase 1- Winter Ontario/Etiwanda

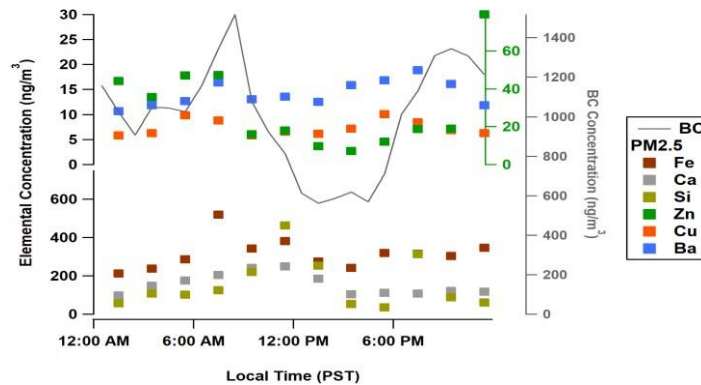
Diurnal profiles of several key elements in PM_{10} and $\text{PM}_{2.5}$ as well as that of BC are shown in Figure 3.14. These figures indicate that.

1. With the sharp increase in BC in the morning, there is a clear morning traffic influence at the site from 5-10 am PST.

2. The increase in crustal elements (especially Si) starts earlier and it doesn't decrease as sharply as BC after 10 am, indicating that the site is not only influenced by on-road, nearby emissions but also it is under the influence of transport of air masses from the western part of the Los Angeles basin.
3. With the increase in boundary layer height and overall reduction in traffic volume, there are lower concentrations of all species mid-day.
4. At around 4 pm, with the afternoon rush hour, there is an increase in BC and several other elements, including Zn and Ba.



(a)



(b)

Figure 3.14 Diurnal profiles of BC and several elements in PM10 (a) and PM2.5 (b) for Phase 1 (Ontario/Etiwanda in Winter 2023).

Phase 3- Summer Rubidoux

Average diurnal profiles of CO, O₃, BC, PM2.5 and PM10 are shown in [Figure 3.15](#).

The peak in primary traffic-related emissions of CO and BC indicate the influence of

local emissions during the morning rush hour as well as significant influence of transport from LA Basin to the site during noon-afternoon timeframe, coinciding with the peak in ozone (a secondary pollutant). Interestingly, PM10 mass shows a stronger morning rush hour peak than PM2.5 and neither shows the large afternoon enhancements like BC or ozone. However, PM2.5 decreases more slowly after the morning peak.

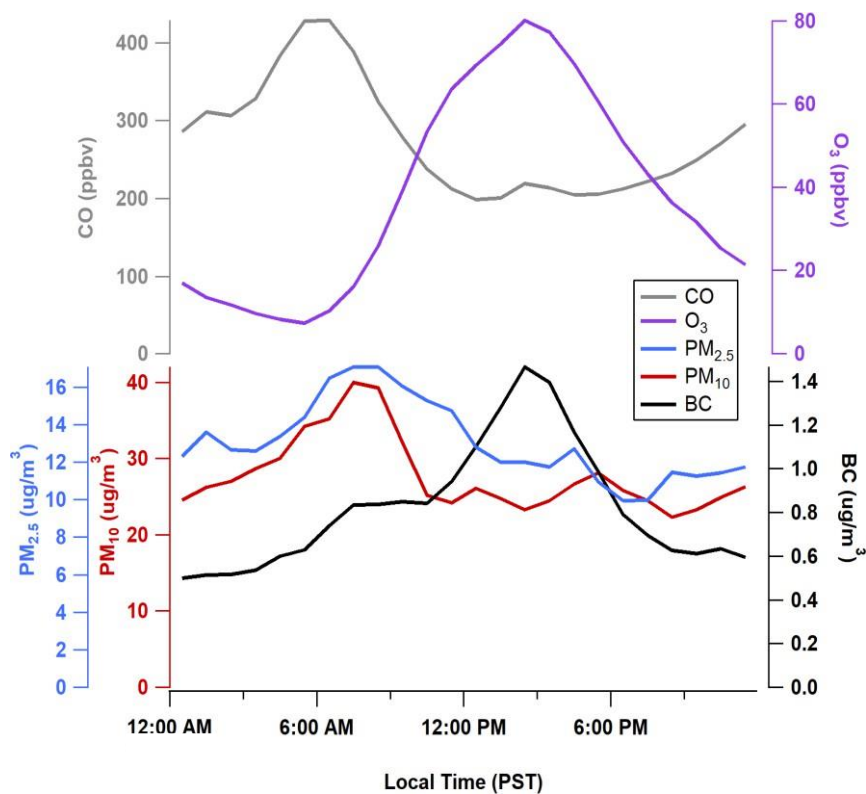


Figure 3.15 Diurnal profiles of PM_{2.5}, PM₁₀, BC, CO, and O₃ for Phase 3 (Rubidoux, in Summer 2023). PM₁₀ data corresponds to the period of deployment of the Xact at Rubidoux (Aug. 25- Sep. 5, 2023) while other data are averages for Aug.- Sep. 2023.

Diurnal profiles of PM₁₀ and PM_{2.5} elements were very similar (Figure 3.16), showing a morning rush hour peak between 4-10 am (PST) and an afternoon peak between 1-8 pm (PST), which coincides roughly with the peak in BC and ozone. For Zn (marker of tire wear emissions), the afternoon peak is as strong as the morning peak, whereas the crustal and brake wear emission tracers have a much weaker afternoon peak.

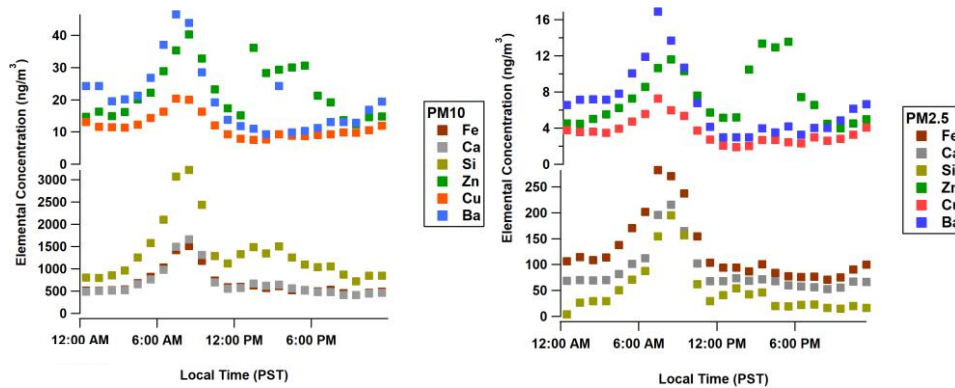


Figure 3.16 Diurnal profiles of several elements in PM10 and PM2.5 during Phase 3 (Rubidoux, Summer).

3.3.4 Source Attributions

Positive Matrix Factorization (PMF) is an established method to determine sources of environmental pollutants in samples based on covariability of pollutant constituents (Frie et al., 2019, 2017; Paatero and Tapper, 1994). In this analysis, the matrix of the observed values of various PM components and trace gases (i.e., X , $n \times m$ dimension) and the corresponding uncertainties (σ , $n \times m$ dimension) are used as input variables. The method solves the following bilinear matrix equation.

$$X = GF + E \quad (3.1)$$

where G is the unknown “factors” ($n \times p$ dimension), F is the unknown associated concentrations of each factor ($p \times m$ dimension), and E is the residual matrix ($n \times m$ dimension). The equation is then solved to minimize the quality of fit, Q , as defined below:

$$Q = \sum_{i=1}^m \sum_{j=1}^n \left(\frac{E_{i,j}}{\sigma_{i,j}} \right)^2 \quad (3.2)$$

The factors and their concentration are in essence the collection of chemical constituents that describe a source profile. The only constrain on the solution is that all elements of G and F are non-negative in order to be physically meaningful, which

makes PMF to be a superior method in its application to environmental sample analysis compared to other factor analysis (e.g., Principal Component Analysis, PCA) (Paatero and Tapper 1994). It is worth noting that the PMF factor profiles derived in each model run are assumed to stay the same throughout the model run, with only their concentrations (i.e., contributions to the total) changing with time.

In this project, concentrations of key elements, plus concentrations of PM10 and/or PM2.5, and auxiliary measurements (BC, CO, and/or O₃) along with their associated uncertainties were used as input parameters to the EPA PMF v5.0 toolkit (available freely online) to determine the source profiles of PM2.5 and/or PM10 (Amato et al., 2016; Farahani et al., 2021). Note that when seeking the PM10 PMF solution, the PM10 elemental composition was used while in PM2.5 PMF solutions, the PM2.5 elemental composition was used. More than two dozen PMF runs for each size fraction have been carried out, with different set of input parameters and numbers of solutions. In determining the best set of solution factors, we considered the trends in the value of Q, stability of the solutions, predictability of the individual input parameters, and physical interpretability of the resolved source factors, based on the known measured chemical characteristics (i.e., fingerprints) of the different components. Too few numbers of solutions will have the influence of several source profiles mixed in together while too many solutions result in splitting of the factors. Below we show the best selection of the PMF results for PM2.5 and PM10 during Phase 1 and Phase 3.

Phase 1- Winter Ontario/ Etiwanda

Figure 3.17 presents results of PMF solution factors across PM10 and PM2.5 elements during Phase 1. In these simulations, we were not able to predict PM10 or PM2.5 concentrations very well (i.e., correlation coefficients (r^2) between the measured input values and PMF predictions were <0.3). It is possible that the location of the two eBAM sensors was not ideal to sample unobstructed air the same way that the Xact instrument was sampling. Therefore, for these PMF runs, only the bi-hourly Xact elemental

concentrations and the concentrations of CO and BC, as tracers of vehicular traffic/combustion processes, were used as inputs. Given the estimated uncertainties in the measurements, As, Cr, and Ni were treated as weak variables in the PM10 PMF runs. On the other hand, for the PM2.5 PMF runs, Cr and Ni were removed because of their frequent very low and uncertain concentrations while Si, Mn, and As were regarded as weak variables.

The best solutions for the PM10 and PM2.5 PMF runs were selected as the 6-factor solution, with convergence on all the tested 50 runs. Furthermore, 100 bootstrapping runs resulted in higher than 83% similarity (defined as $r > 0.6$) between its results and solutions of the base run, and displacement runs did not show any error or rotational ambiguity in the solutions. Similarly, for the PM2.5 PMF runs, all the tested 50 runs converged; the 100 bootstrapping runs showed more than 84% similarity, and displacement runs did not show any error or solution ambiguity.

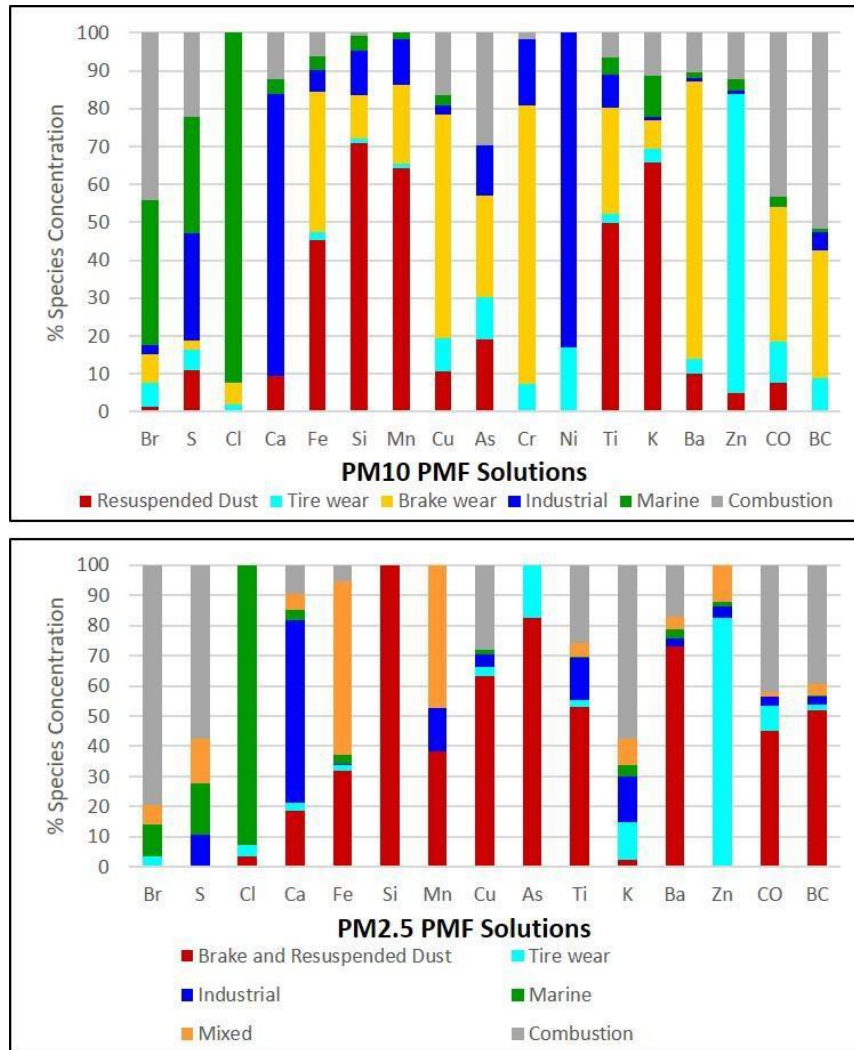


Figure 3.17 Distribution of different PM10 and PM2.5 PMF solutions across different elements during Phase 1 (Ontario/Etiwanda, Winter).

When interpreting both the PM10 and PM2.5 sets of solutions, “Brake Wear” and “Tire Wear” factors were assigned based on the respective dominance of Ba and Zn in the factors. For PM10, the assignment for the “Resuspended Dust” factor was based on the high contribution of several crustal elements such as Si, Mn, Ti, K and Fe. However, in the PM2.5 set of solutions, crustal elements were grouped mainly with Ba; therefore, we believe here the Brake Wear factor also has influence of “Resuspended Dust”. The “Marine” factors in both size fractions show significant contribution to Cl, and to some extent to S and Br. In PM10, the “Industrial” factor has a strong contribution to Ni (but

also Ca, which is unusual, but could indicate influence from a specific industry). In PM2.5, we did not have a good detection of Si; however, the “Industrial” factor has a strong contribution to Ca again with additional contributions to other elements (e.g., Mn, Ti, Cu, S). The factor interpreted as “Combustion” explains 40-50% of BC and CO which are markers for incomplete fuel combustion.

Phase 3- Summer Rubidoux

Figure 3.18 highlights the distribution of different PMF solution factors across PM10 and PM2.5 elements during Phase 3. All species shown in these figures were used as input variables in the PMF. In solving for the PM10 factors, As, Cr, and Ni were treated as weak variables; all the tested 50 runs converged; 100 bootstrapping runs resulted in more than 80% similarity between its results and solutions of the base run; furthermore, displacement runs did not show any error or rotational ambiguity in the solutions. When solving the PM2.5 factors, As, Si, Mn, and PM2.5 were treated as weak variables. The reason for setting the PM2.5 mass concentration as weak is that PM2.5 is not over-emphasized by PMF because of inclusion of aerosol organics and nitrate (available from ASCENT measurements) which are the two dominant components of PM2.5. Similar to PM10 solutions, all the tested 50 runs converged; the 100 bootstrapping runs showed more than 74% similarity, and displacement runs did not show any error or solution ambiguity. It is worth noting that while the PM10 PMF model is based on ~10 days of available PM10 elemental data, the PM2.5 PMF model is based on a 2-month (Aug.- Sep. 2023) data available from ASCENT in order to improve predictability of the PMF model.

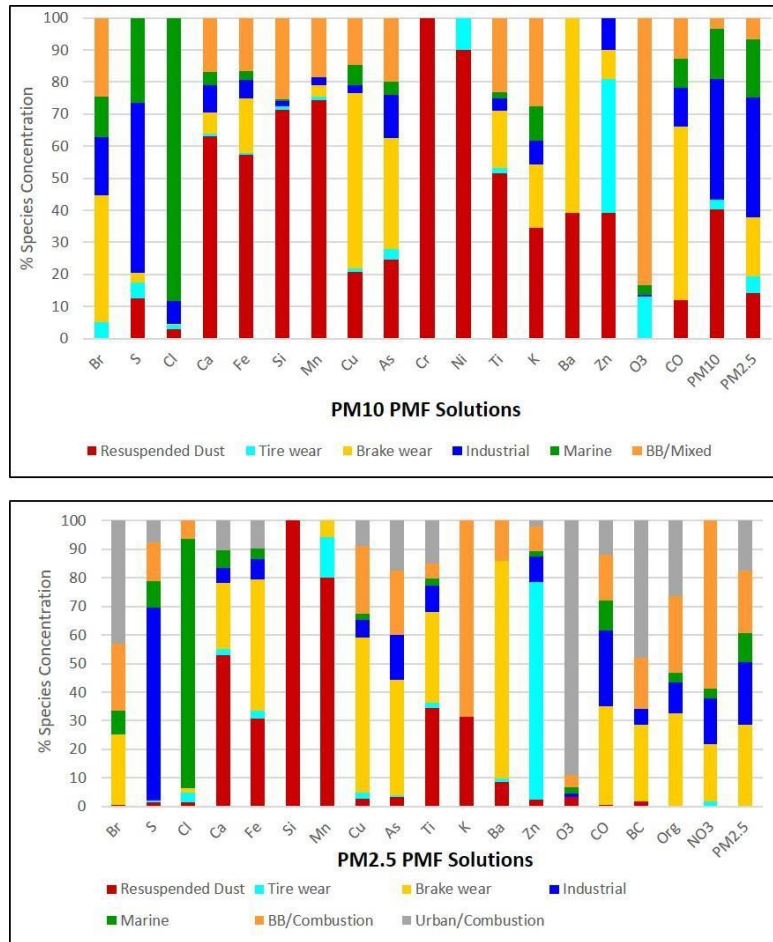


Figure 3.18 Distribution of different PM10 and PM2.5 PMF solutions across different elements during Phase 3 (Rubidoux, Summer).

In both sets of solutions, the factor enriched in crustal elements such as Ca, Si, Mn, Ti is called “Resuspended Dust;” the factors dominating Ba and Zn respectively are identified as “Brake wear” and “Tire Wear.” Note that in the PM10 solution set, 40% of Zn is also associated with the “Resuspended Dust” factor, suggesting that this factor also includes some signatures of rubber. This could be from rubberized asphalt that is used on some roads in LA Basin or from tire wear particles that are mixed in with Resuspended dust and cannot be well separated by PMF. However, as outlined in the next section, we can estimate only the crustal mass associated with the Resuspended Dust factor to better isolate its contribution to PM. Other factors identified based on their elemental abundance are “Marine” because of high contribution to Cl; “Industrial”

due to high contribution to S, combustion markers like CO, and anthropogenic elements such as As; “BB/Mixed”, “BB/Combustion” or “Urban/Combustion” sources due to contributions from primary and secondary biomass or fossil fuel combustion products (K, O3, CO, BC).

3.3.5 Overall Assessment of Contribution of Road Dust to PM₁₀ and PM_{2.5}

Because of the location of our sampling sites and potential contribution of natural dust emissions from arid areas in the Inland Empire, it is possible that the PMF cannot separate out contribution of crustal material from road dust vs. arid lands. We therefore proceed to reconstruct the mass concentration of crustal material associated with the PMF-Road Dust factors and consider its diurnal profiles to estimate the contribution of traffic-related crustal material to PM₁₀ and PM_{2.5}.

The IMPROVE network has developed an empirical formula (Eq. 3.3) to estimate the total mass of crustal material based on measurements of the main elements of soil, namely, Al, Ca, Fe, Ti, and Si, to account for the mass of the main soil minerals containing these elements (Pettijohn, 1975):

$$\text{Crustal Material} = 2.2 \times \text{Al} + 1.63 \times \text{Ca} + 2.42 \times \text{Fe} + 1.94 \times \text{Ti} + 2.49 \times \text{Si} \quad (3.3)$$

However, Xact measurements of Al are typically uncertain unless high concentrations are measured. Therefore, we used the ratio of Al to Ca (determined as the slope of a scatter plot of Al vs. Ca when the measured Al concentration to its uncertainty was greater than 1) and substituted the corresponding values in PM₁₀ (Al/Ca=0.70 ± 0.06 for Phase 3) and PM_{2.5} (Al/Ca=1.26 ± 0.04 for Phase 3) for the first term in Eq. 3.3. Furthermore, we used the fractional attribution of Ca, Fe, Ti, and Si to the Resuspended Dust factor solution of PM₁₀ and PM_{2.5} when calculating the crustal material mass. These attributions are summarized in [Table 3.2](#).

Table 3.2 Summary of Resuspended Dust attributions to Ca, Fe, Ti, and Si in PM10 and PM2.5 PMF solutions during Phase 3 (Rubidoux, Summer).

% of Species In “Resuspended Dust”	PM10	PM2.5
Ca	63.07	52.99
Fe	57.22	30.87
Ti	51.56	34.61
Si	71.38	100

Results of these calculations for Phase 3 are presented in [Figure 3.19](#). These figures demonstrate that crustal materials are ~10% of background PM10 and 2% of background PM2.5. Furthermore, we can attribute the observed increase due to local or transported traffic-related activities relative to the background as the resuspended crustal material from roads alone. Based on these profiles, traffic/road-related crustal material is 15% of PM10 and 12% of PM2.5. These estimates agree reasonably well with the resuspended dust contributions to PM10 and PM2.5 in the Greater Boston Area as reported by Matthaios et al. (17.5% and 9.1% for PM10 and PM2.5, respectively) (2022).

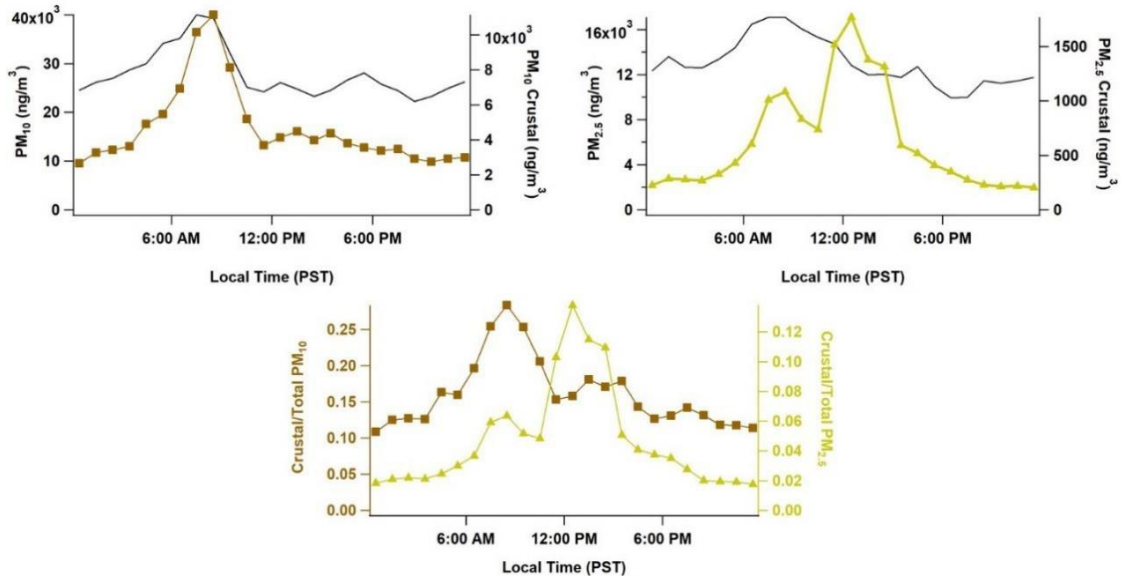


Figure 3.19 Diurnal profiles of PM_{10} , $PM_{2.5}$, and calculated crustal mass of PM_{10} and $PM_{2.5}$ during Phase 3 (Rubidoux, Summer).

3.3.6 Emission Factors of Road Crustal Material, Brake Wear, and Tire Wear

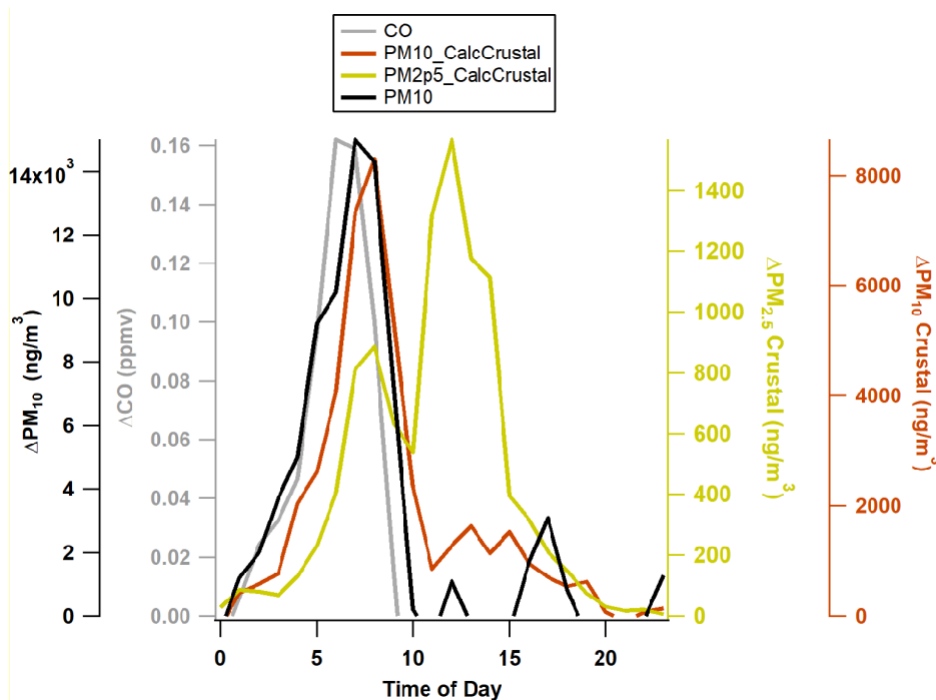


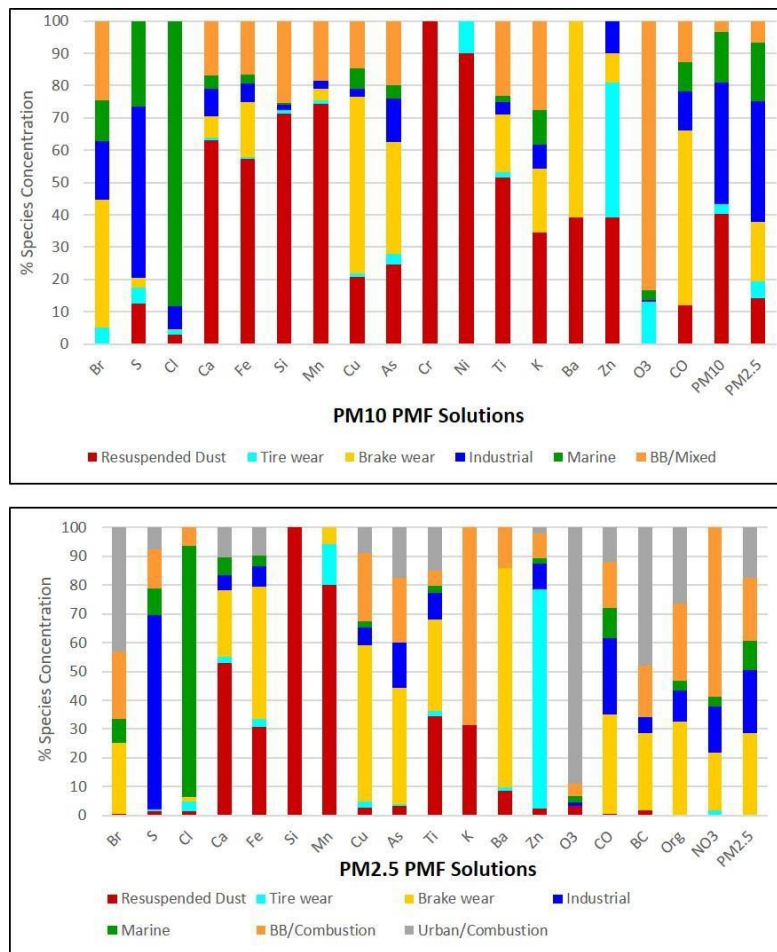
Figure 3.20 Diurnal profiles of PM_{10} , CO, crustal mass of PM_{10} and $PM_{2.5}$ during Phase 3 (Rubidoux, Summer). Early morning background values are subtracted so that enhancements during morning rush hour (5-10 am) can be considered as the traffic related emissions.

To estimate the total emission factor of the crustal material portion of the PM, the enhancements observed in the PM₁₀ or PM_{2.5}-calculated crustal material and CO over the background are combined with the emission factor of CO for the average fleet in California in the following equations:

$$EF_{Crustal\ Material} = \frac{\Delta Crustal\ PM}{\Delta CO} \times \frac{\varnothing}{VMT} \quad (3.4)$$

Using the early morning peaks in $\Delta Crustal\ PM_{10}$ (8200 ng/m³) and $\Delta Crustal\ PM_{2.5}$ (865 ng/m³) (Figure 3.20), peak ΔCO of 0.16 ppmv (Figure 3.20), and CO/VMT of 0.922 g CO per vehicle miles travelled (CARB, 2022), the estimated $EF_{PM_{10}\ Crustal\ Material}$ and $EF_{PM_{2.5}\ Crustal\ Material}$ are 41.5 mg/VMT and 4.4 mg/VMT, respectively. These are average emission factors that represent emissions in the South Coast Air Basin, upwind of Rubidoux, with the average 2020-2024 California fleet of light duty passenger vehicles, light duty trucks, and motorcycles (CARB, 2022).

Based on the PM10 PMF results at Rubidoux, ~3% of PM₁₀ is attributed to Tire wear



(Top Panel in

Figure 3.18). Therefore, based on the morning peak in ΔPM_{10} ($15,000 \text{ ng/m}^3$, Figure 3.20), the peak $\Delta \text{Tire wear } PM_{10}$ is estimated to be 450 ng/m^3 , leading to $EF_{PM_{10} \text{ Tire wear}}$ of 2.3 mg/VMT . The PM10 PMF runs did not attribute any brake wear aerosol to the measured PM10, likely due to its low contribution or uncertainties in PMF in separating the Brake wear elements from resuspended dust. However, based on the

PM10 Brake wear factor contribution to PM2.5 mass (~20%, Top Panel of

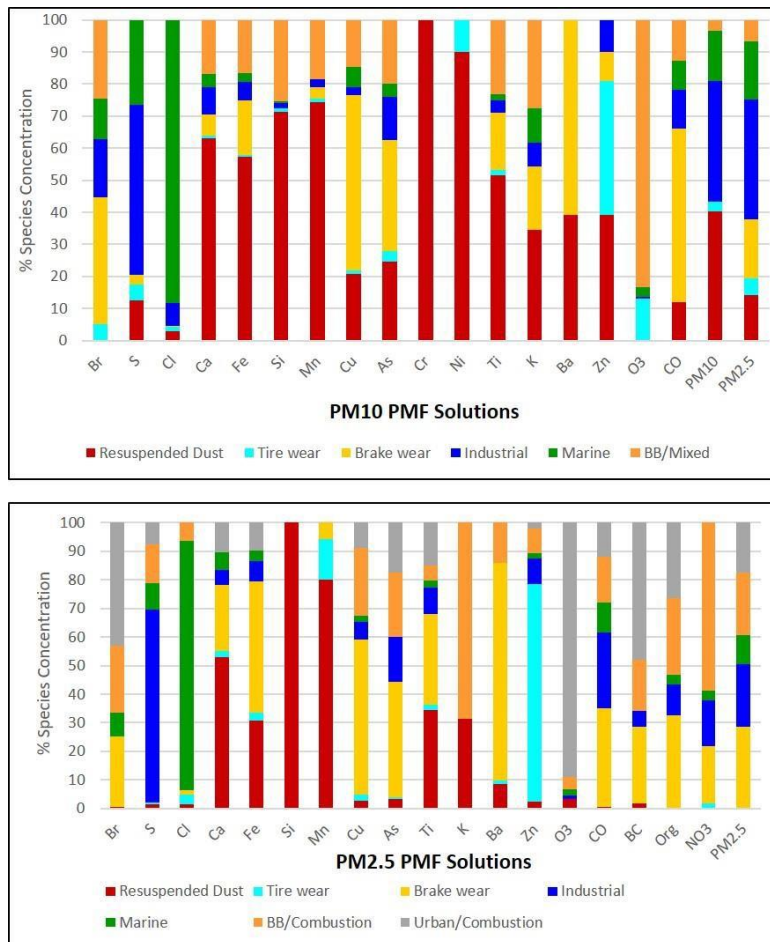


Figure 3.18) and the observed fraction of PM10 that is PM2.5 (0.36 ± 0.05), the peak $\Delta_{Brake\ wear\ PM10}$ is estimated to be 1080 ng/m^3 , leading to a rough estimate of EF_{PM10} Brake wear of 5.5 mg/VMT .

References

- Amato, F., Cassee, F.R., Denier van der Gon, H.A.C., Gehrig, R., Gustafsson, M., Hafner, W., Harrison, R.M., Jozwicka, M., Kelly, F.J., Moreno, T., Prevot, A.S.H., Schaap, M., Sunyer, J., Querol, X., 2014. Urban air quality: The challenge of traffic non-exhaust emissions. *J. Hazard. Mater.* 275, 31–36. <https://doi.org/10.1016/j.jhazmat.2014.04.053>
- Amato, F., Favez, O., Pandolfi, M., Alastuey, A., Querol, X., Moukhtar, S., Bruge, B., Verlhac, S., Orza, J.A.G., Bonnaire, N., Le Priol, T., Petit, J.-F., Sciare, J., 2016. Traffic induced particle resuspension in Paris: Emission factors and source contributions. *Atmos. Environ.* 129, 114–124. <https://doi.org/https://doi.org/10.1016/j.atmosenv.2016.01.022>
- Barkjohn, K. K., Gantt, B., & Clements, A. L. (2021). Development and application of a United States-wide correction for PM 2.5 data collected with the PurpleAir sensor. *Atmospheric Measurement Techniques*, 14(6), 4617-4637.
- Caltrans, 2020. Pems User Guide Table of Contents.
- Casotti Rienda, I., Alves, C.A., 2021. Road dust resuspension: A review. *Atmos. Res.* 261. <https://doi.org/10.1016/j.atmosres.2021.105740>
- Denier van der Gon, H., Hulskotte, J., Jozwicka, M., Kranenburg, R., Kuenen, J., Visschedijk, A., 2018. European Emission Inventories and Projections for Road Transport Non-Exhaust Emissions, Non-Exhaust Emissions: An Urban Air Quality Problem for Public Health; Impact and Mitigation Measures. Elsevier Inc. <https://doi.org/10.1016/B978-0-12-811770-5.00005-4>
- Farahani, V.J., Soleimanian, E., Pirhadi, M., Sioutas, C., 2021. Long-term trends in concentrations and sources of PM_{2.5}-bound metals and elements in central Los Angeles. *Atmos. Environ.* 253. <https://doi.org/10.1016/j.atmosenv.2021.118361>
- Frie, A.L., Dingle, J.H., Ying, S.C., Bahreini, R., 2017. The Effect of a Receding
-
- UCR/ME-80014-MR-2-R0 82 College of Engineering

- Saline Lake (The Salton Sea) on Airborne Particulate Matter Composition.
Environ. Sci. Technol. <https://doi.org/10.1021/acs.est.7b01773>
- Frie, A.L., Garrison, A.C., Schaefer, M.V., Bates, S.M., Botthoff, J., Maltz, M., Ying, S.C., Lyons, T., Allen, M.F., Aronson, E., Bahreini, R., 2019. Dust sources in the Salton Sea Basin: A clear case of an anthropogenically impacted dust budget.
Environ. Sci. Technol. <https://doi.org/10.1021/acs.est.9b02137>
- Matthaios, V.N., Lawrence, J., Martins, M.A.G., Ferguson, S.T., Wolfson, J.M., Harrison, R.M., Koutrakis, P., 2022. Quantifying factors affecting contributions of roadway exhaust and non-exhaust emissions to ambient PM_{10-2.5} and PM_{2.5-0.2} particles. *Sci. Total Environ.* 835, 155368.
<https://doi.org/10.1016/j.scitotenv.2022.155368>
- OECD, 2020. Non-exhaust Particulate Emissions from Road Transport, Non-exhaust Particulate Emissions from Road Transport. <https://doi.org/10.1787/4a4dc6ca-en>
- Paatero, P., Tapper, U., 1994. Positive Matrix Factorization - a Nonnegative Factor Model with Optimal Utilization of Error-Estimates of Data Values.
Environmetrics 5, 111-12.
- Pettijohn, F.J., *Sedimentary Rocks*, 2nd Edition, Harper & Row Publishers, New York, 1975.
- Reid, S., Bai, S., Du, Y., Craig, K., Erdakos, G., Baringer, L., Eisinger, D., McCarthy, M., Landsberg, K., 2016. Emissions modeling with MOVES and EMFAC to assess the potential for a transportation project to create particulate matter hot spots. *Transp. Res. Rec.* 2570, 12–20. <https://doi.org/10.3141/2570-02>
- Snyder, M.G., Venkatram, A., Heist, D.K., Perry, S.G., Petersen, W.B., Isakov, V., 2013. RLINE: A line source dispersion model for near-surface releases. *Atmos. Environ.* 77. <https://doi.org/10.1016/j.atmosenv.2013.05.074>
- Thiruvengkatahari, R.R., Ding, Y., González-Rocha, J., Carranza, V., Rojas Robles,

N., Hopkins, F., Venkatram, A., 2023. Estimating inputs for dispersion modeling in mobile platform applications. *Sci. Total Environ.* 881, 163306.
<https://doi.org/10.1016/j.scitotenv.2023.163306>

US EPA (United States Environmental Protection Agency). 1993. Procedures For Sampling Surface/Bulk Dust Loading. Last Modified January 01, 1995. Accessed December 01, 2024. <https://www.epa.gov/sites/default/files/2020-11/documents/app-c1.pdf>.

US EPA (United States Environmental Protection Agency). 2011a. AP-42 Background Documentation. Last Modified January 01, 2011. Accessed December 01, 2024. https://www.epa.gov/sites/default/files/2020-10/documents/emission_factor_documentation_for_ap-42_section_13.2.1_paved_roads_.pdf. US EPA (United States Environmental Protection Agency). 2011b. AP 42 Chapter 13: Miscellaneous Sources. *English*. Vol. Volume I. Last Modified January 01, 2011. Accessed December 01, 2024. https://www.epa.gov/sites/production/files/2020-10/documents/13.2.1_paved_roads.pdf. US EPA, 1995. Procedures for laboratory analysis of surface/bulk dust loading samples.

US EPA (United States Environmental Protection Agency). 2011b. AP 42 Chapter 13: Miscellaneous Sources. *English*. Vol. Volume I. Last Modified January 01, 2011. Accessed December 01, 2024. https://www.epa.gov/sites/production/files/2020-10/documents/13.2.1_paved_roads.pdf

Venkatram, A., 2008. Computing and displaying model performance statistics. *Atmos. Environ.* 42, 6862–6868. <https://doi.org/10.1016/j.atmosenv.2008.04.043>

Venkatram, A., 2000. A critique of empirical emission factor models: A case study of the AP- 42 model for estimating PM10 emissions from paved roads. *Atmos. Environ.* 34. [https://doi.org/10.1016/S1352-2310\(99\)00330-1](https://doi.org/10.1016/S1352-2310(99)00330-1)

Venkatram, A., Fitz, D., Bumiller, K., Shuming, D., Boeck, M., Ganguly, C., 1999.
Using a dispersion model to estimate emission rates of particulate matter from
paved roads. *Atmos. Environ.* 33, 1093–1102. [https://doi.org/10.1016/S1352-2310\(98\)00316-1](https://doi.org/10.1016/S1352-2310(98)00316-1)

Venkatram, A., Schulte, N., 2018. *Urban Transportation and Air Pollution*, Elsevier.
Joe Hayton.

Appendix A: Electronic Data Files for Dust Project

All source data from this study have been stored in a [cloud database](#). The folder labeled "2023" contains experimental data collected during the summer of 2023, while the "2024" folder includes data from experiments conducted in 2024.